



Simulation models



This project has received funding from the European Union's Horizon 2020 research and innovation programme under grant agreement No 883985

Table of contents

Table of contents	2
List of figures.....	4
List of Acronyms.....	7
Summary	8
EMT and Phasor Simulation.....	9
1.1 EMT simulation.....	10
1.1 Phasor simulation.....	11
2 The VSC Model.....	14
2.1 EMT and Phasor simulation	14
2.2 VSC model mask	15
2.3 VSC Electrical part	17
2.4 VSC Control block.....	18
2.4.1 abc to dq transformation	19
2.4.2 Control loops	21
2.4.2.1 Control loops – SW, AVG and Phasor QEMT	22
2.4.2.2 Control loops – Phasor I-1st.....	24
2.4.2.3 Control loops – Phasor I-ref.....	25
2.4.2.4 Control loops – Phasor PQ-1st	26
2.4.3 Modulation block (dq to abc transformation)	27
2.4.3.1 Modulation block – EMT SW	27
2.4.3.2 Modulation block – EMT AVG	28
2.4.3.3 Modulation block – Phasor QEMT.....	28
2.4.3.4 Modulation block – Phasor I-1st, Phasor I-ref and Phasor PQ-1 st	30
3 Synchronous generator model.....	31
3.1 Electrical model.....	31
3.2 Control system	32
3.2.1 Speed governor model.....	33
3.2.2 Exciter system model.....	34
4 Case studies – VSC model.....	36
4.1 Setpoint tracking	37
4.1.1 PLL	37
4.1.2 Current-controller.....	37

4.1.3	Power-controller	38
4.2	Load and generation variations	39
4.2.1	Load change.....	39
4.2.2	Voltage variation	39
4.2.3	Frequency variation	40
4.3	Frequency droop	40
4.4	Voltage droop	41
4.5	Symmetrical fault + LVRT	42
4.6	Asymmetrical fault + negative sequence control.....	44
4.7	Discussion	45
5	Case studies – HV system	46
5.1	Load variation.....	47
5.2	Loss of generation	48
5.3	Symmetrical fault.....	50
5.4	Asymmetrical fault	52
5.5	Line outage.....	54
6	References.....	55

List of figures

Figure 1 – Time frame of several transients in power systems [4].....	9
Figure 2 – a) Inductor. b) Inductor Norton equivalent.....	11
Figure 3 – AC voltage magnitude step in an RL circuit.....	12
Figure 4 – AC voltage magnitude step in an RL circuit. Phasor solution multiplied by $\exp(j\omega t)$	12
Figure 5 – EMT simulation chosen in powergui.....	14
Figure 6 – Phasor simulation chosen in powergui.....	15
Figure 7 - VSC model top layer.....	15
Figure 8 – VSC mask options.....	15
Figure 9 – VSC mask initialization function window.....	16
Figure 10 – VSC mask internal blocks.....	16
Figure 11 – VSC model variant subsystem.....	17
Figure 12 – Electrical part of the VSC SW model.....	17
Figure 13 – Electrical part of the VSC AVG model.....	18
Figure 14 – Electrical part of the VSC Phasor model.....	18
Figure 15 – Inside the VSC Control block.....	18
Figure 16 – Variant subsystems inside the Measurements block of VSC control block.	19
Figure 17 – EMT measurements block: PLL + dq transformation.....	19
Figure 18 – PLL aligned with positive sequence v_d	20
Figure 19 – Phase sequence separation using DSC method.....	20
Figure 20 – abc to dq transformation in the Phasor models.....	21
Figure 21 – Variant subsystems used in the control loops block.....	22
Figure 22 – Inside the detailed control loops block in VSC control.....	22
Figure 23 – PQ calculation considering negative sequence components.....	23
Figure 24 – Outer loop in control.....	23
Figure 25 – Inner loop in the detailed control loops block.....	24
Figure 26 – Inner loop approximated by a first-order transfer function in the Phasor I-1st model.....	25
Figure 27 – Outer loop modified considering the elimination of the inner loop in the Phasor I-ref model.....	26
Figure 28 – Outer loop approximated by a first-order transfer function in the Phasor PQ-1st model.....	26
Figure 29 – Variant subsystems inside the Modulation block.....	27
Figure 30 – SW model modulation.....	28
Figure 31 – AVG model dq to abc transformation.....	28
Figure 32 – Phasor QEMT model abc to dq transformation.....	29
Figure 33 – Adding RL time constant to Phasor QEMT model output reference.....	29
Figure 34 – Phasor I-1st ,I-ref and PQ-1st Modulation block.....	30
Figure 35 – SG model d-axis equivalent circuit [9].....	31
Figure 36 – SG model q-axis equivalent circuit [9].....	31
Figure 37 – Modelled SG in Simulink.....	33
Figure 38 – Subsystems that compose the SG model.....	33

Figure 39 – Speed governor model.....	34
Figure 40 – Exciter system model.	34
Figure 41 – Transducer and load compensation model.	34
Figure 42 – PSS model.....	35
Figure 43 – Exciter model.	35
Figure 44 – Simulated system.....	36
Figure 45 – Modelled synchronous generator.	37
Figure 46 – PLL initialization.	37
Figure 47 – Output-current setpoint tracking.	38
Figure 48 – Active power setpoint tracking.	38
Figure 49 – Reactive power setpoint tracking.	38
Figure 50 – Converter AC power during load change.....	39
Figure 51 – Converter AC power during a voltage variation.	39
Figure 52 – Generator speed during a sudden load increase.	40
Figure 53 – Converter power during a frequency variation.	40
Figure 54 – Frequency during a load increase with VSC droop.....	41
Figure 55 – Converter output power during a frequency variation.	41
Figure 56 – AC voltage during voltage droop test.	42
Figure 57 – Converter output reactive power during voltage droop test.	42
Figure 58 – AC voltage magnitude during the three-phase fault.	42
Figure 59 – Reactive current injection provided by the LVRT.	43
Figure 60 – Generator current during the three-phase fault.	43
Figure 61 – Generator current during the three-phase fault, detail on the first instants of the fault.....	43
Figure 62 – Generator speed during the fault.	44
Figure 63 – Converter positive and negative sequence dq currents during the asymmetrical fault.	44
Figure 64 – Converter positive and negative sequence dq voltages during the asymmetrical fault.	45
Figure 65 – Converter average AC power output during the asymmetrical fault.	45
Figure 66 – Test system diagram.	46
Figure 67 – HV test system modelled in Simulink.	47
Figure 87 - SMs speeds during a load connection. VSC connected.	47
Figure 88 - SMs speeds during a load connection (detail). VSC connected.	48
Figure 89 – SMs speeds during outage of G1. VSC connected.	48
Figure 90 – SMs speeds during outage of G1 (detail). VSC connected.	49
Figure 91 – SMs torques during outage of G1. VSC connected.	49
Figure 92 – SMs torques during outage of G1 (detail). VSC connected.	49
Figure 93 – VSC output AC power during outage of G1 (detail). VSC connected.	50
Figure 94 - SMs speeds during an symmetrical fault. VSC connected.	50
Figure 95 - SMs speeds during an symmetrical fault (detail). VSC connected.	51
Figure 96 - SMs torques during an symmetrical fault (detail). VSC connected.	51
Figure 97 - Converter voltage magnitude during a symmetrical fault. VSC connected.	51
Figure 98 - Converter positive and negative sequence dq currents during a symmetrical fault. VSC connected.	52
Figure 99 - SMs speeds during an asymmetrical fault. VSC connected.	52

Figure 100 - SMs speeds during an asymmetrical fault (detail). VSC connected.....	53
Figure 101 - SMs torques during an asymmetrical fault (detail). VSC connected.....	53
Figure 102 - Converter positive and negative sequence dq currents during an asymmetrical fault. VSC connected.....	53
Figure 103 - SMs speeds during a line outage. VSC connected.....	54
Figure 104 - SMs speeds during a line outage (detail). VSC connected.....	54
Figure 105 - SMs torques during a line outage (detail). VSC connected.	54

List of Acronyms

EMT	Electromagnetic Transients
EMTP	Electromagnetic Transients Program
KCL	Kirchhoff's Current Law
KVL	Kirchhoff's Voltage Law
ODE	Ordinary Differential Equation
PSS	Power System Stabilizer
SEXS	Simplified Exciter System
SG	Synchronous Generator
SP	Static Phasor
TS	Transient Stability
VSC	Voltage Source Converter

Summary

This report describes the components and models developed in Task 1.5 of WP1. It serves as an introduction to the Simulink and Matlab files sent to the members of the consortium.

EMT and Phasor Simulation

Most electrical power systems are composed of machines, transmission lines, loads, passives elements, switching elements and non-linear elements. Each element can be modelled in multiple ways, considering a very detailed model or a simpler one. The model is often chosen depending on the type of study to be performed, the phenomena being analyzed and the available computational power. For example, in a typical Transient Stability (TS) study, where the dynamics typically slow, it would not be necessary to use detailed transmission line models, such as [1], and transformer models such as [2], since in this frequency range the simple models provide sufficiently accurate responses. However, detailed models are necessary when simulating Very Fast Front Transients, which have dynamics in the MHz range [3]. Several time frames of typical power systems studies are depicted in Figure 1.

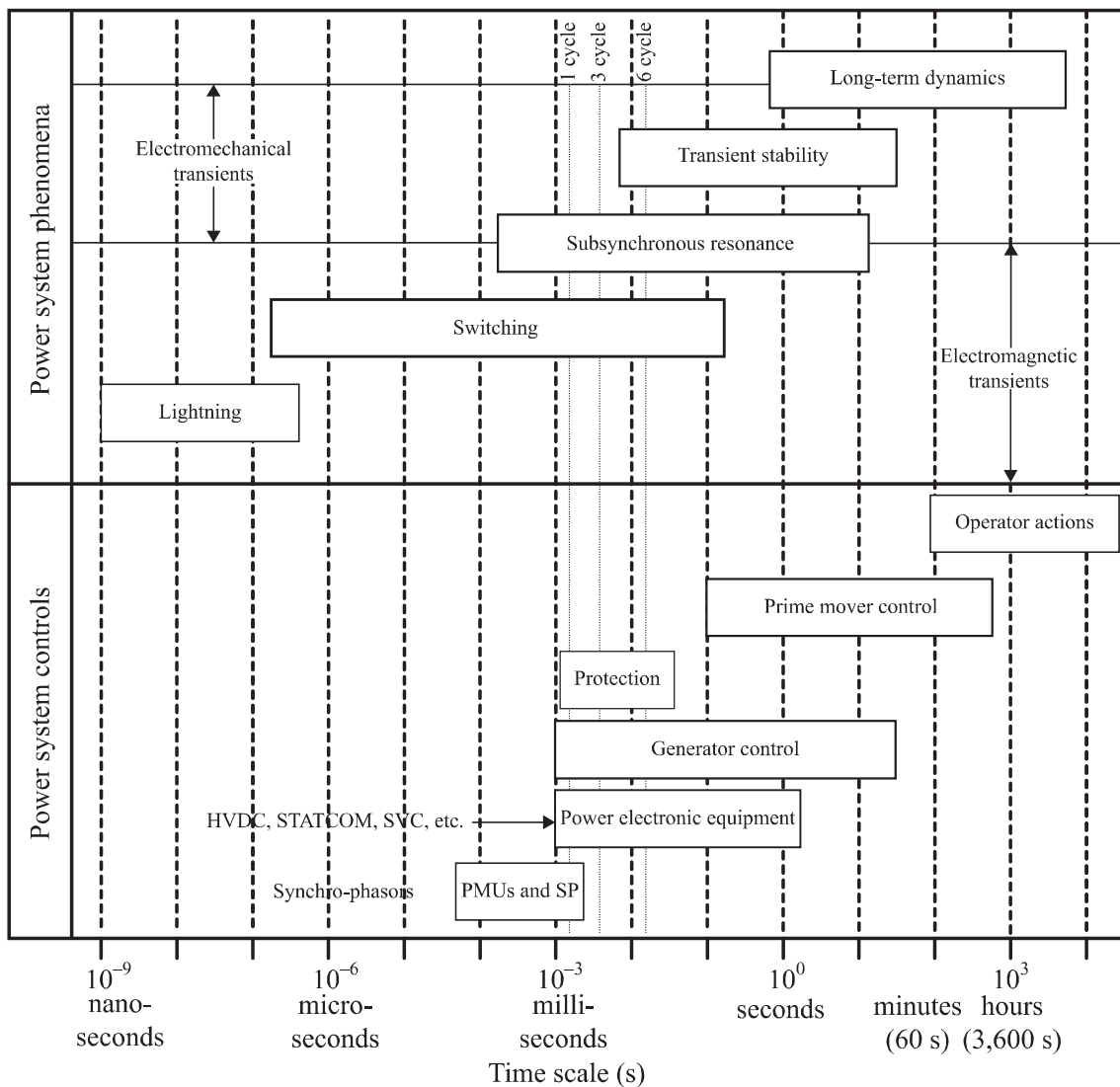


Figure 1 – Time frame of several transients in power systems [4].

The different modelling approaches also comprise the domain (time or frequency) the system under study will be simulated. The typical approaches to simulate power systems in the time-domain are the ones based on Electromagnetic Transients (EMT) or Phasors, which are briefly introduced next.

1.1 EMT simulation

The EMT solution comprises a set of ordinary differential equations (ODEs) based on Kirchhoff's Current and Voltage laws (KCL and KVL, respectively). This set of ODEs describes the circuit's complete response when subjected to a voltage or current [4].

There are several numerical methods to solve ODEs. One largely used in power systems is the method proposed by H. W. Dommel of Bonneville Power Administration. The method was called EMTP (Electromagnetic Transients Program) [5] and was based on the difference equations model obtained with the trapezoidal rule. Several well-known commercial and non-commercial programs are based on the original EMTP and on its improvements, such as ATP, PSCAD, EMTP-RV, RTDS, HYPERSIM and PowerFactory. After decades of validations and improvement, the EMTP method is the most generally accepted method to perform EMT simulations [4]. The principle of the method is to apply a numerical integrator substitution method, such as the trapezoidal integrator, discretizing the system components given a predetermined time-step and combining the discretized elements into a single matrix.

The EMTP method is exemplified next for an inductor.

Using the notation of Figure 2a, the differential equation for the inductor is:

$$v_L = v_k - v_m = L \frac{di_{km}}{dt} \quad (1)$$

Transforming (1) into an integral equation we have:

$$i_{km}(t) = i_{km}(t - \Delta t) + \int_{t-\Delta t}^t (v_k - v_m) dt \quad (2)$$

Applying the trapezoidal rule gives:

$$\begin{aligned} i_{km}(t) &= i_{km}(t - \Delta t) + \frac{\Delta t}{2L} ((v_k(t) - v_m(t)) + (v_k(t - \Delta t) - v_m(t - \Delta t))) \\ &= i_{km}(t - \Delta t) + \frac{\Delta t}{2L} (v_k(t - \Delta t) - v_m(t - \Delta t)) + \frac{\Delta t}{2L} (v_k(t) - v_m(t)) \\ &= I_{hist}(t - \Delta t) + \frac{1}{R_{eff}} (v_k(t) - v_m(t)) \end{aligned} \quad (3)$$

Writing (3) in the form shown in the last line has the especial advantage of representing the equation in the form of a Norton equivalent, as illustrated in Figure 2b. In this equivalent circuit, the current source (I_{hist}) represents the current from the previous time-step (history term) and the conductance $1/R_{eff}$ represents the current

contribution at the present time-step to a voltage at the present time-step. A similar approach can be performed to the resistor and the capacitor.

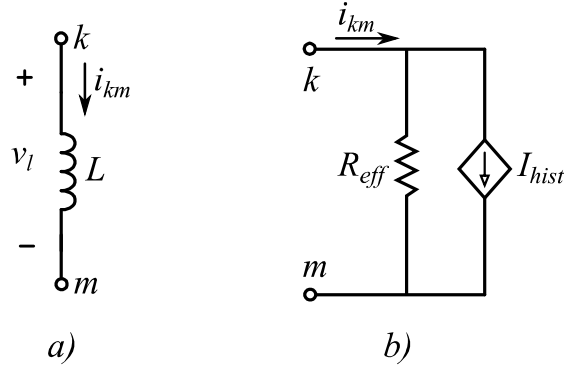


Figure 2 – a) Inductor. b) Inductor Norton equivalent.

It should be noted that different parameters of the Norton equivalent are obtained if another numerical integrator substitution method is used (e.g., Backward Euler).

After transforming each element to an equivalent circuit, well-known circuit analysis methods can be used to solve the circuit, such as circuit reduction and network solution techniques. EMTP uses a nodal formulation to solve the system:

$$\mathbf{Gv(t)} = \mathbf{i(t)} + \mathbf{I}_{hist} \quad (4)$$

Where \mathbf{G} is the conductance matrix, $\mathbf{v(t)}$ is the vector of nodal voltages, $\mathbf{i(t)}$ is the vector of external current sources and \mathbf{I}_{hist} is the vector of current sources representing the historical terms.

Further information about the complete solution process can be found in [6, 4, 7, 8]

1.1 Phasor simulation

The Phasor solution assumes a steady-state condition at the power frequency. This implies that the frequency of voltages and currents throughout the system is nearly constant, varying slowly. Therefore, the passive elements are transformed into impedances or admittances calculated at the power frequency and the system network is solved considering a constant admittance matrix (\mathbf{Y}_{bus}) [9]:

$$\mathbf{Y}_{bus}\mathbf{V} = \mathbf{I} \quad (5)$$

Where, \mathbf{Y}_{bus} is the bus admittance matrix, \mathbf{V} is the bus voltage vector and \mathbf{I} is the bus current injection vector.

Among the benefits of phasor models are the simpler models used in the simulation, which requires fewer parameters to be known, and the possibility of using larger simulation time-steps, which greatly decrease the simulation time. One of the

drawbacks is the limited range of studies that can be accurately performed in phasor simulations given that only slow dynamics are accurately represented.

Now, similar to what was performed for the EMT model, the inductor equation in the phasor model is:

$$I = \frac{1}{jw_s L} V \quad (6)$$

Where w_s is the power frequency in rad/s.

Transforming (1) to the frequency domain we have:

$$I(s) = \frac{1}{sL} V(s) + \frac{1}{s} i(0) \quad (7)$$

Now, comparing (6) with (7) it can be observed that the EMT model represents the inductor for any arbitrary frequency s subject to an arbitrary excitation $V(s)$ and represents the inductor initial current $i(0)$. On the other hand, the phasor model assumes a constant frequency w_s and does not account for the initial current value.

The differences between both models are highlighted in Figure 3 and Figure 4, where an AC voltage of 50 Hz is applied to an RL circuit, with 0.5 V in $t = 0$ and with 1.0 V in $t = 0.5$ s. The circuit parameters were $R = 1 \Omega$ and $L = 100 \text{ mH}$.

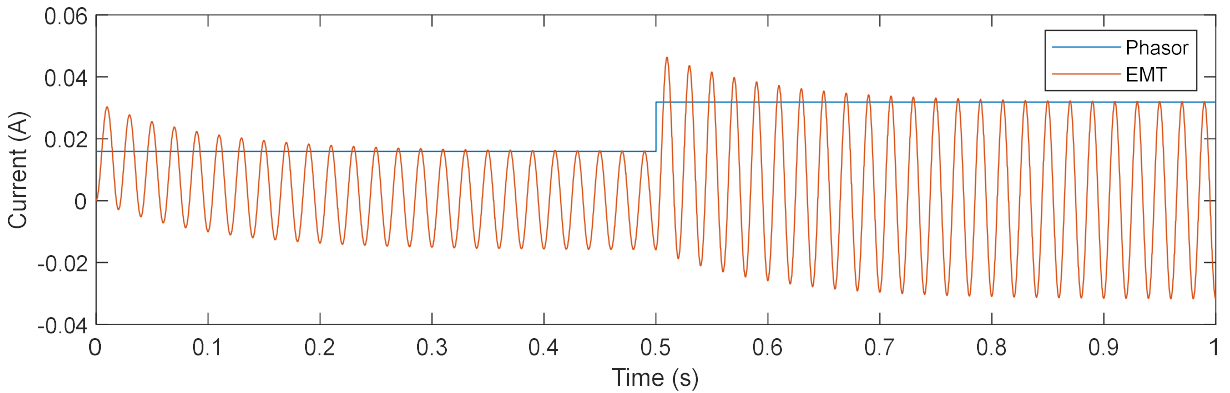


Figure 3 – AC voltage magnitude step in an RL circuit.

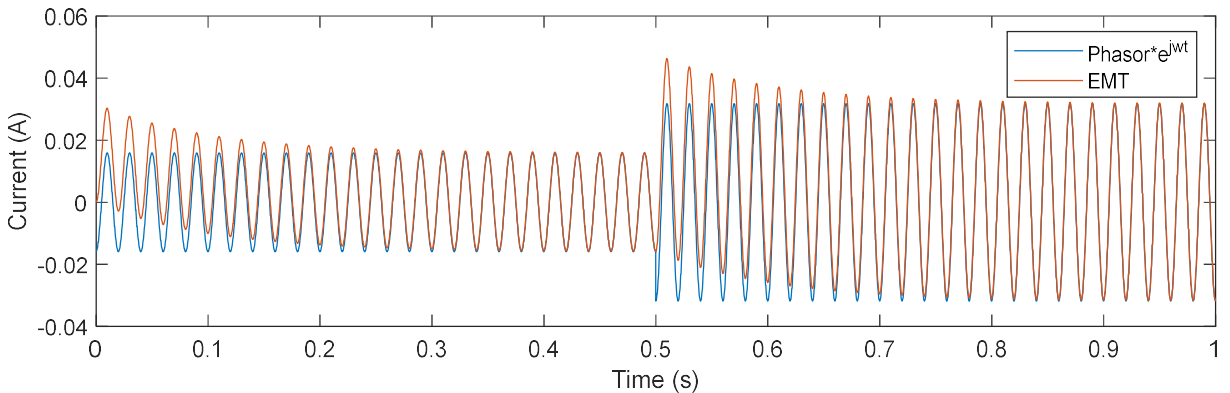


Figure 4 – AC voltage magnitude step in an RL circuit. Phasor solution multiplied by $\exp(j\omega t)$.

As can be observed in Figure 4, the phasor and EMT models match in the steady-state at the power frequency value, but the phasor model does not represent the DC exponential decaying component imposed by the RL time constant.

2 The VSC Model

This section describes the modelled VSC in Simulink using six different models, including two EMT models: Switching model (SW) and Average Model (AVG), and four phasor models: Quasi-EMT (QEMT), Current loop first order (I-1st), Current loop reference (I-ref) and power-loop first order (PQ-1st). They are summarized in Table 1.

Table 1 – Implemented VSC models in Simulink.

Name	Characteristic	Fastest dynamics
EMT SW	Switching model	PWM
EMT AVG	EMT Average model	Current loop
Phasor Quasi-EMT	Detailed Phasor model	Current loop
Phasor I-1st	Current loop controller substituted by a first-order transfer function $(i_{dq} = F(s) * i_{dqref})$	Current loop
Phasor I-ref	Current loop eliminated $(i_{dq} = i_{dqref})$	Power loop
Phasor PQ-1st	Current loop eliminated and power loop controller substituted by a first-order transfer function $(PQ = F(s) * PQref)$	Power loop

The particularities of each model are presented next in this section.

2.1 EMT and Phasor simulation

Both SW and AVG models are simulated in the time domain, and the Phasor models are simulated in the frequency domain (limited only to the power frequency, 50 Hz or 60 Hz). The simulation type (EMT or Phasor) must be chosen in the powergui block located in the Simulink model, as below.



Figure 5 – EMT simulation chosen in powergui.

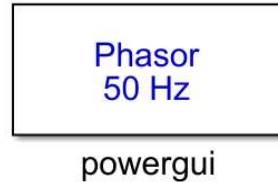


Figure 6 – Phasor simulation chosen in powergui.

2.2 VSC model mask

The top layer of the VSC modelled in Simulink is depicted in Figure 7.

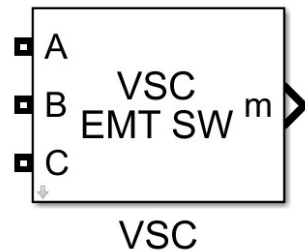


Figure 7 - VSC model top layer.

In the model, “ABC“ represent the three-phase electrical connection to the grid and “m“ the measured and calculated signals inside the model, which can be accessed using a bus selector block in Simulink.

The VSC block is a mask that presents the following options for parameters:

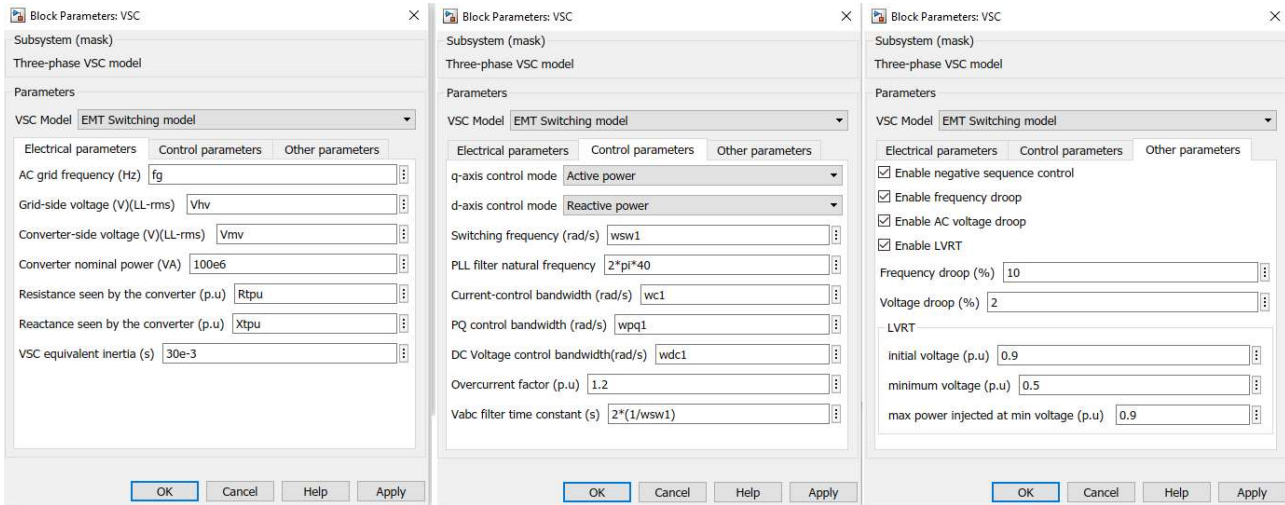


Figure 8 – VSC mask options.

Six options are available for the VSC model: SW, AVG, Phasor QEMT, Phasor I-1st, Phasor I-ref and Phasor PQ-1st. For each option, specific parameters are visible or invisible. For example, the switching frequency parameter is visible only in the SW model.

When the model is simulated, a callback function is executed inside the mask which calculates the required parameters, variables and constants used by the VSC model (Figure 9).

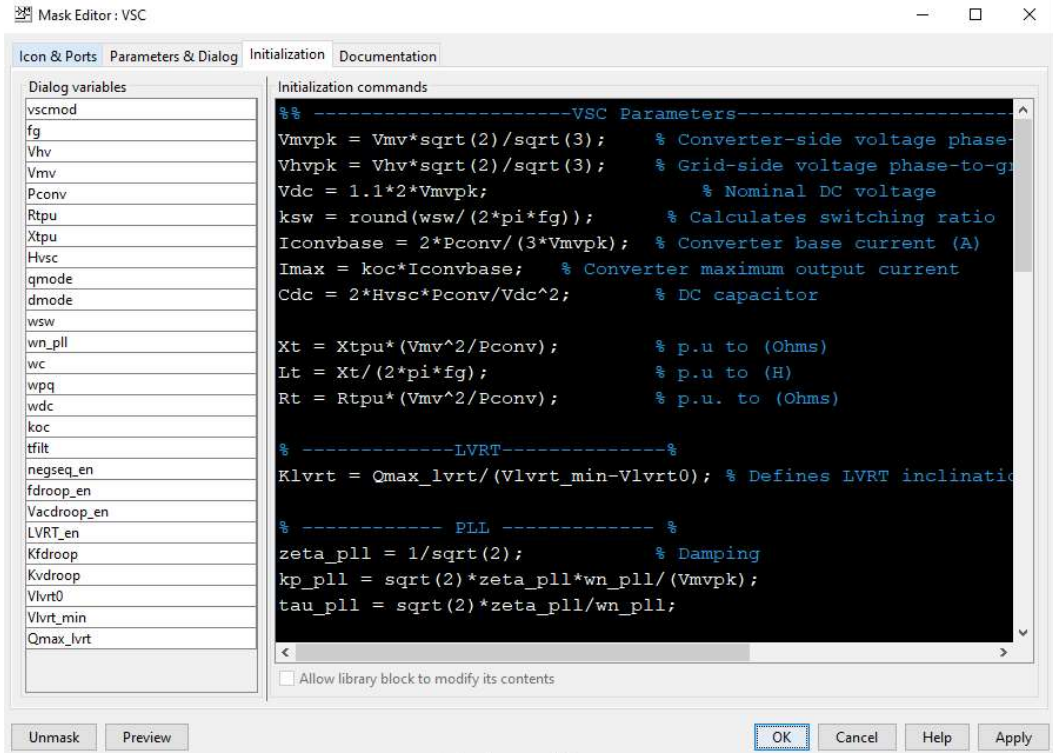


Figure 9 – VSC mask initialization function window.

When entering in the VSC mask, the following blocks can be found (Figure 10):

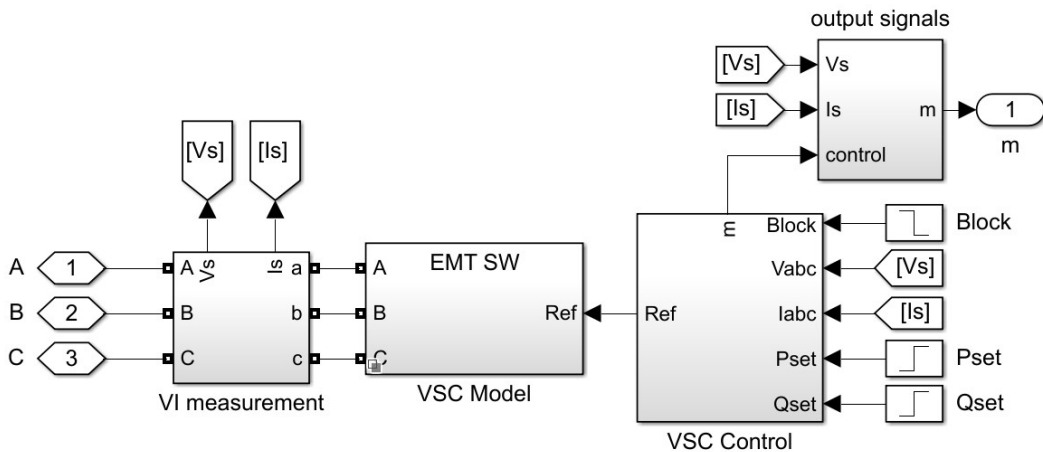


Figure 10 – VSC mask internal blocks.

The VI measurement block measures phase-to-ground voltages and line currents (convention positive current from ABC to abc). If EMT simulation is chosen in the powergui block, the measured voltages and currents will be real variables in the time domain. If Phasor simulation is chosen, voltages and currents will be measured as complex variables.

The *Output signals* block prepares the measured and calculated variables to be output outside the mask.

2.3 VSC Electrical part

The VSC Model block contains the converter electrical part for each model type (SW, AVG or Phasor). This is a variant subsystem block, which ensures that only one of the models is simulated (SW in the example of Figure 11).

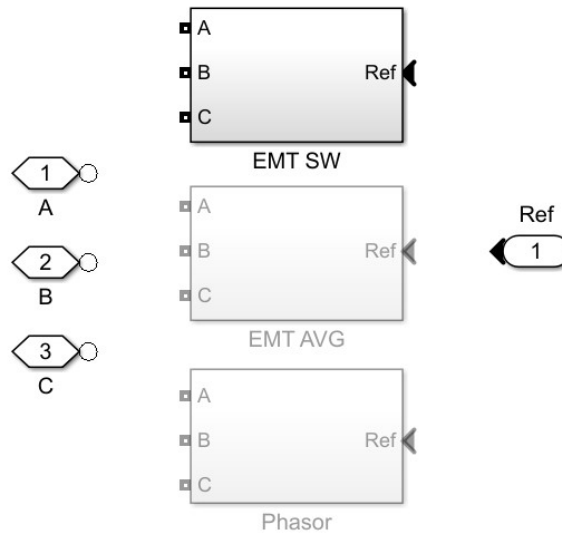


Figure 11 – VSC model variant subsystem.

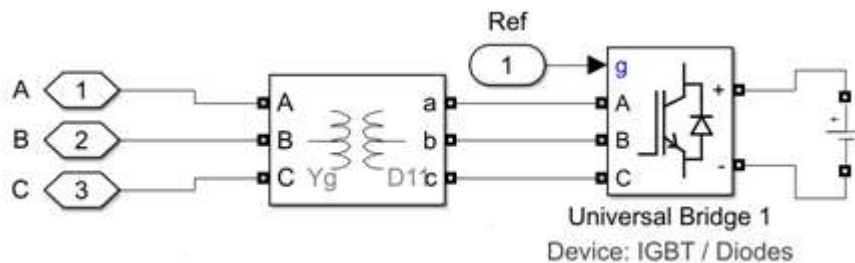


Figure 12 – Electrical part of the VSC SW model.

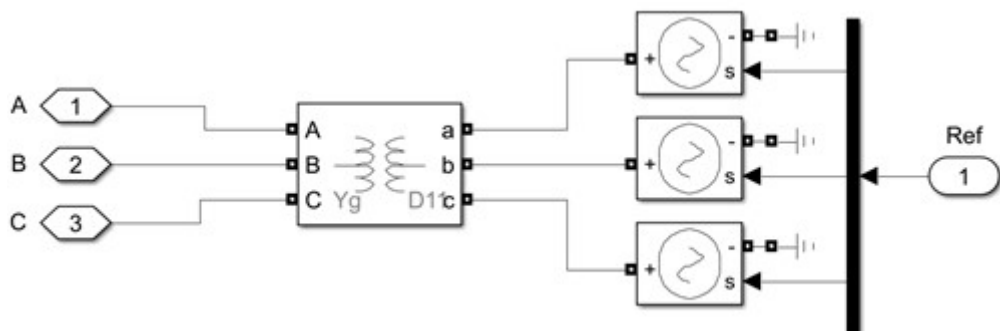


Figure 13 – Electrical part of the VSC AVG model.

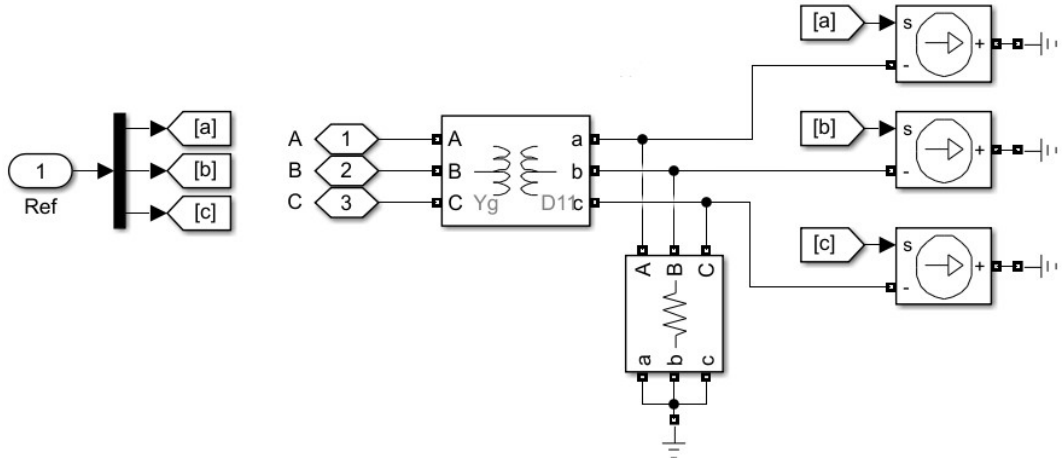


Figure 14 – Electrical part of the VSC Phasor model.

The electrical part of the SW model is represented by a three-phase connection of IGBTs and diodes connected to an ideal DC voltage source. To increase the fidelity, the ideal DC voltage source can be substituted by a DC capacitor charged, for example, by a PV or a wind farm through a DC link.

The electrical part of the AVG model consists of three dependent voltage sources controlled by the Ref signal generated by the control.

The electrical part of the Phasor models consists of three dependent current sources. A snubber is connected to the current sources to avoid numerical issues in the case of open circuits.

The Ref signal represents the pulses in the SW model, the three-phase voltages in the AVG model and the three-phase currents in the Phasor models.

2.4 VSC Control block

The VSC Control block is composed of three blocks: Measurements, Control and Modulation.

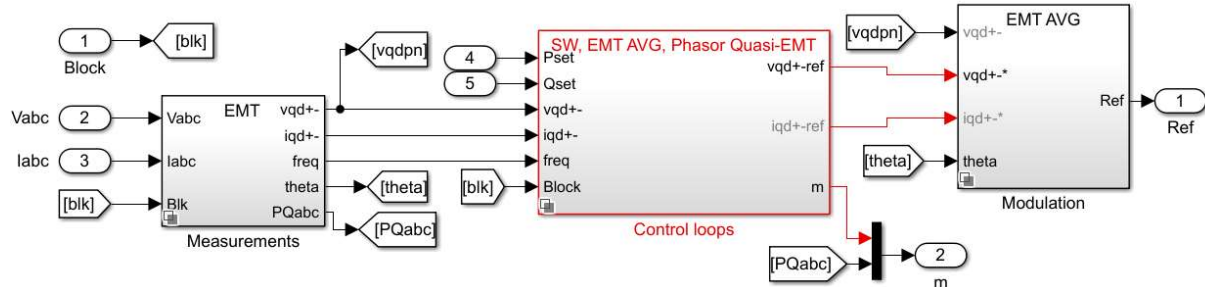


Figure 15 – Inside the VSC Control block.

2.4.1 abc to dq transformation

The Measurements block transforms the measured voltages and currents from the *abc* to the *dq* axis. Both EMT models (SW and AVG) share the same blocks and use PLL while the Phasor models do not require PLL.

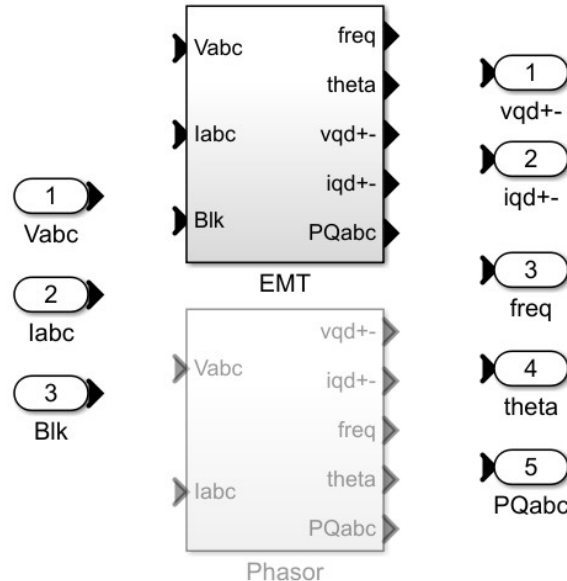


Figure 16 – Variant subsystems inside the Measurements block of VSC control block.

The EMT SW model has a first-order low-pass filter with cut-off frequency equal to the VSC switching frequency, to filter high-frequency noise.

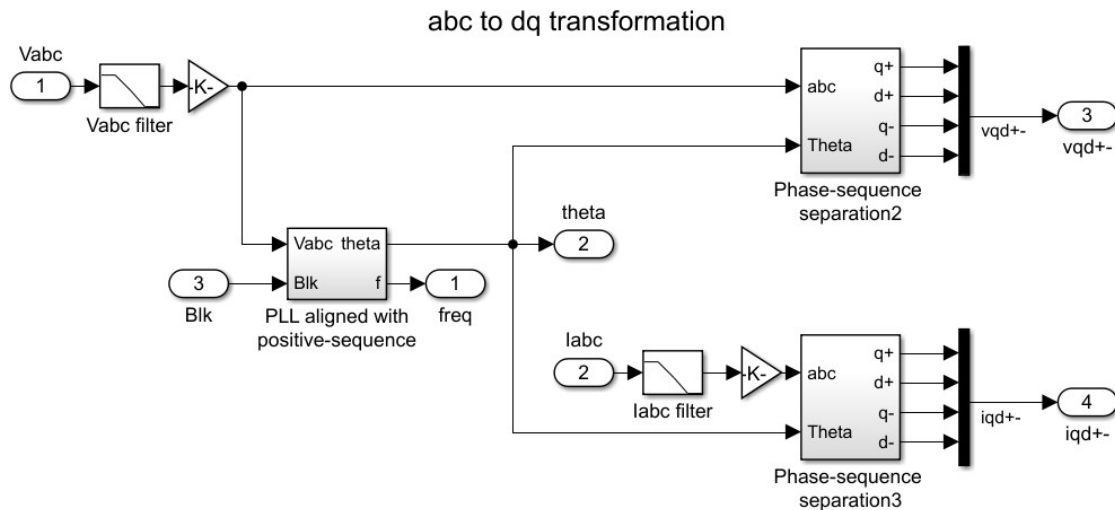
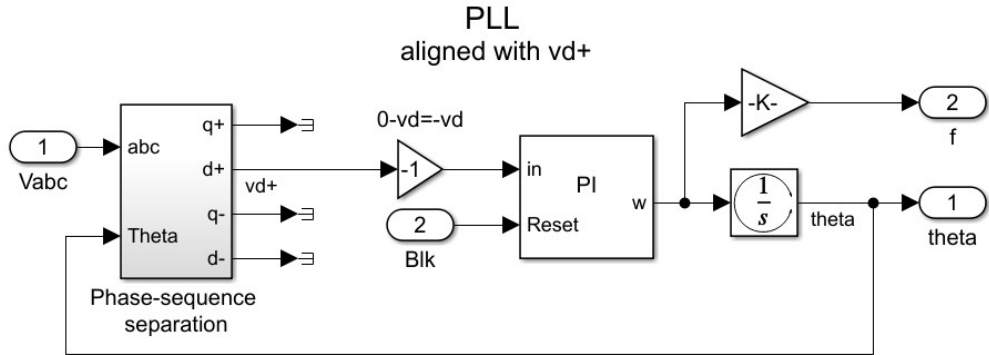


Figure 17 – EMT measurements block: PLL + dq transformation.

The VSC control was implemented for both positive and negative sequence variables. The PLL was implemented aligned with the positive sequence v_d .

Figure 18 – PLL aligned with positive sequence v_d .

The sequence separation in the time domain can be performed by several methods. In this study, the Delayed Signal Cancellation (DSC) was used. However, as the performance of the DSC reduces in off-nominal frequency conditions, notch filters can also be used.

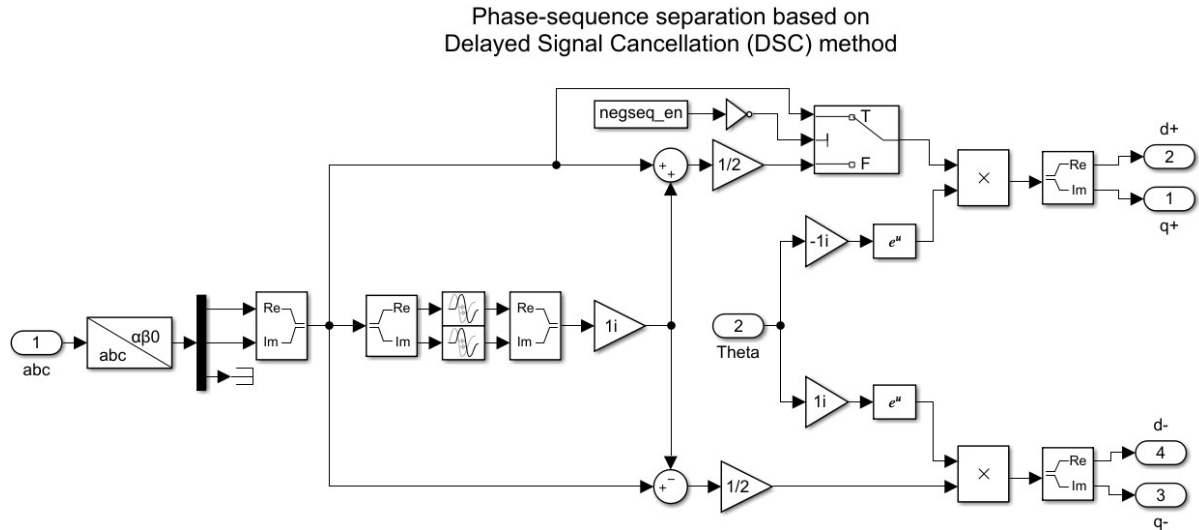


Figure 19 – Phase sequence separation using DSC method.

In the Phasor models, sequence separation is straightforward when using Fortescue transformation. After the phase variables are transformed to sequence components, the dq components are obtained by shifting the sequence variables in phase using the phase of the voltage of phase A (v_a). This phase shifting represents the ideal operation of the PLL.

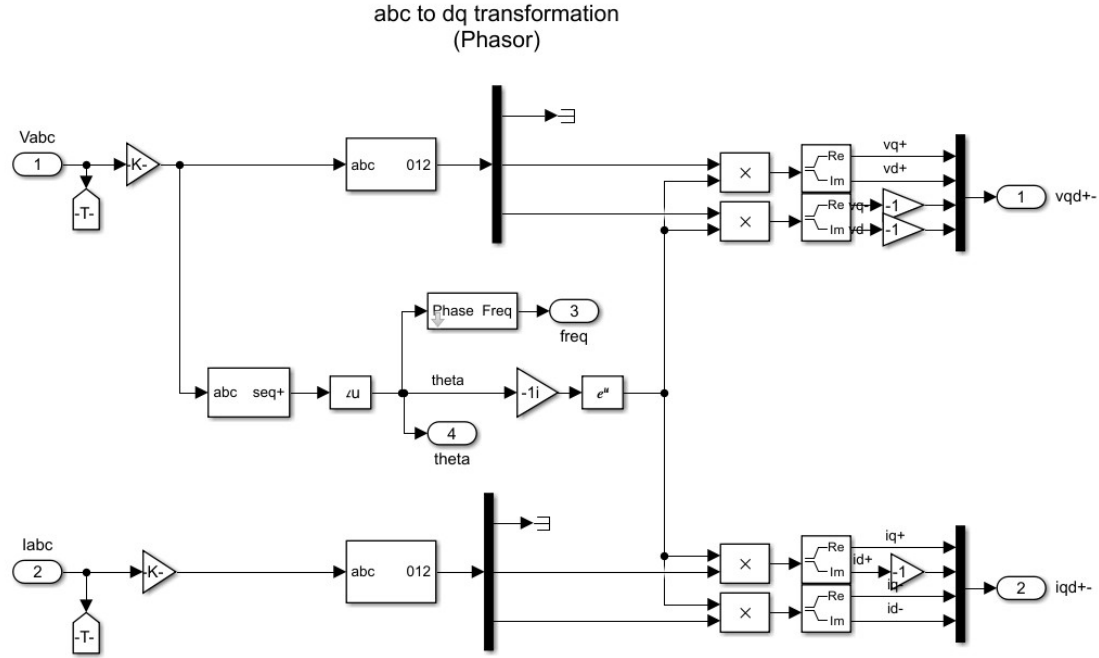


Figure 20 – abc to dq transformation in the Phasor models.

2.4.2 Control loops

After calculating the positive and negative sequence components of voltages and currents in the dq axis, these variables are used in the control loops.

This block was also modelled using variant subsystems. The complete control loops are used by the models EMT SW, EMT AVG and Phasor QEMT. The other subsystems are approximations of this detailed one. Each approximation is discussed next.

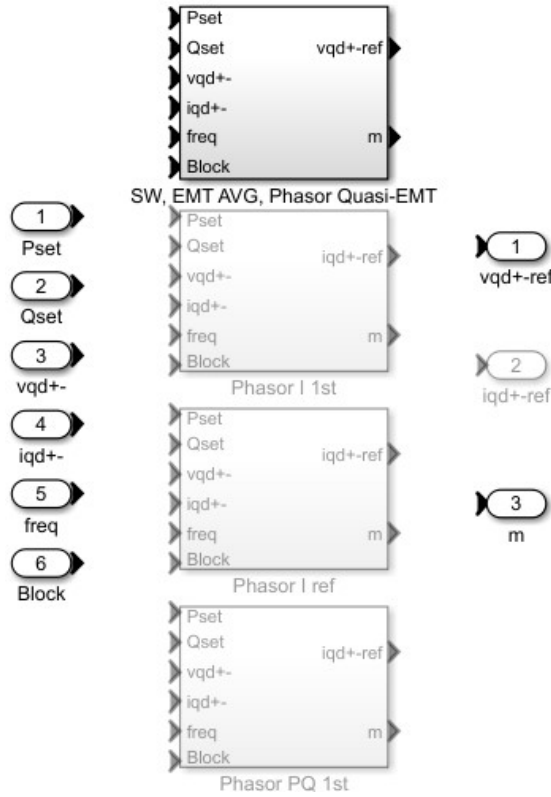


Figure 21 – Variant subsystems used in the control loops block.

2.4.2.1 Control loops – SW, AVG and Phasor QEMT

The control loops block is exactly the same for the models EMT SW, EMT AVG and Phasor QEMT. It consists of an outer loop that controls power and/or voltage and defines current references for the inner loop. The inner loop defines the required voltage to produce the desired current.

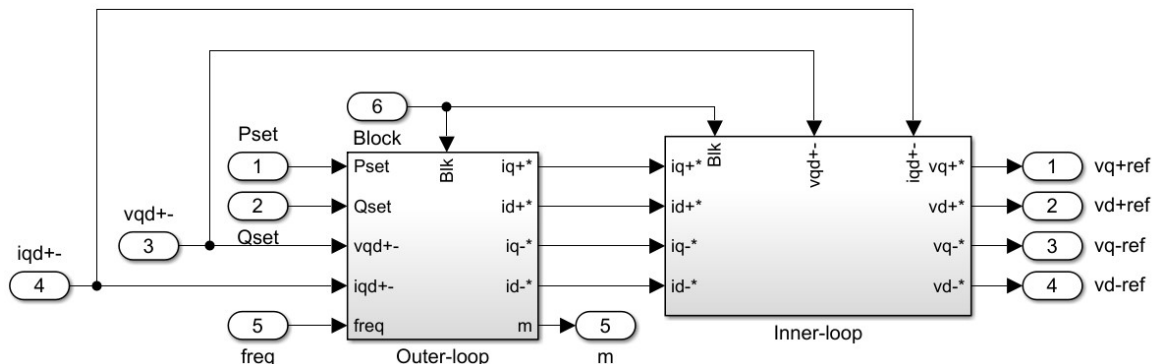


Figure 22 – Inside the detailed control loops block in VSC control.

Inside the outer-loop, the first block is the power calculation block. This block calculates the active and reactive powers considering the presence of negative sequence components in the system.

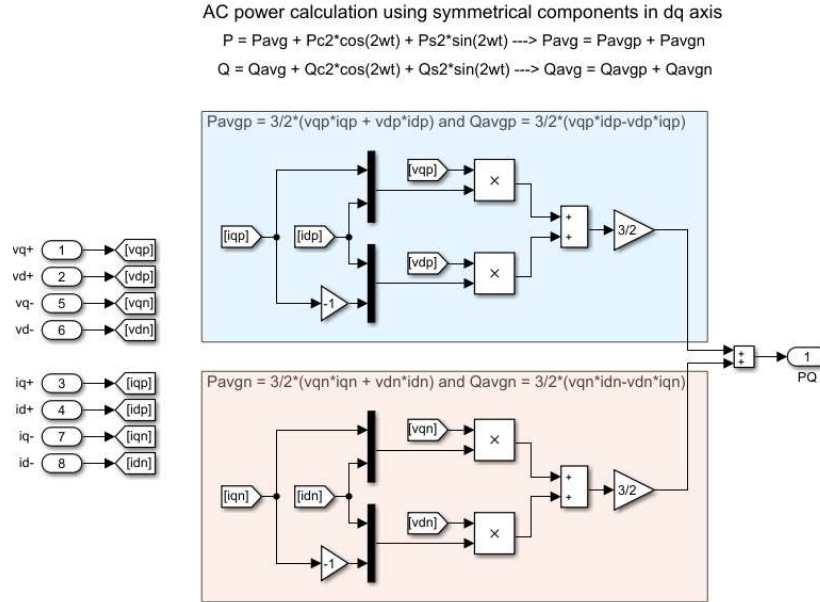


Figure 23 – PQ calculation considering negative sequence components.

As the chosen control strategy was to control the negative sequence currents to zero and control the average active and reactive powers, these power components are used in the control.

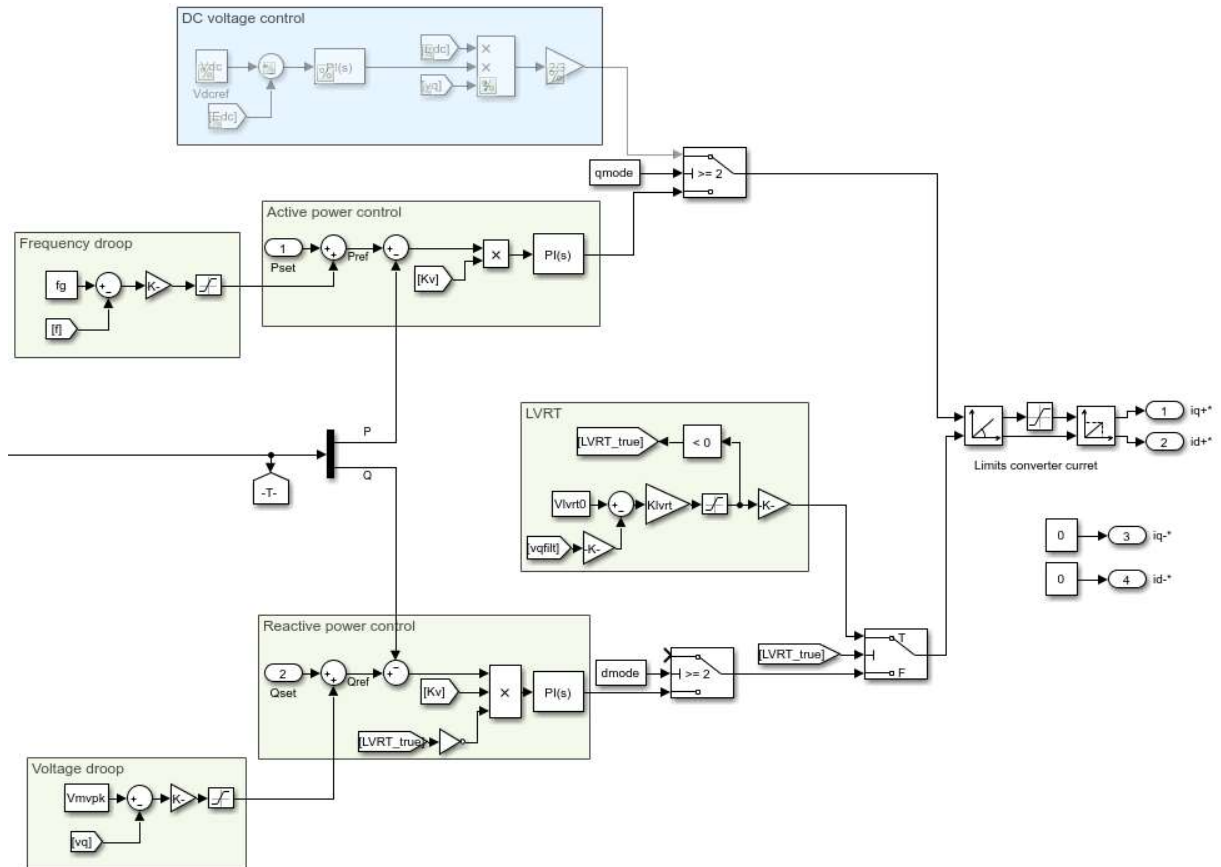


Figure 24 – Outer loop in control.

When controlling the active and reactive power, the power reference is defined by the setpoint (P_{set} and Q_{set}) summed to the voltage droop, in reactive power, and by the frequency droop, in the active power. When there is a fault, the LVRT characteristic is activated and the i_d reference is calculated directly by the LVRT block. **Note the 'capacitor-like' convention used in the models: negative power means power being injected into the grid.**

The reference values for positive and negative dq currents are passed to the inner loop. The inner loop is composed of a positive-sequence current control and a negative sequence control which define the reference values for the positive and negative sequence voltages, respectively.

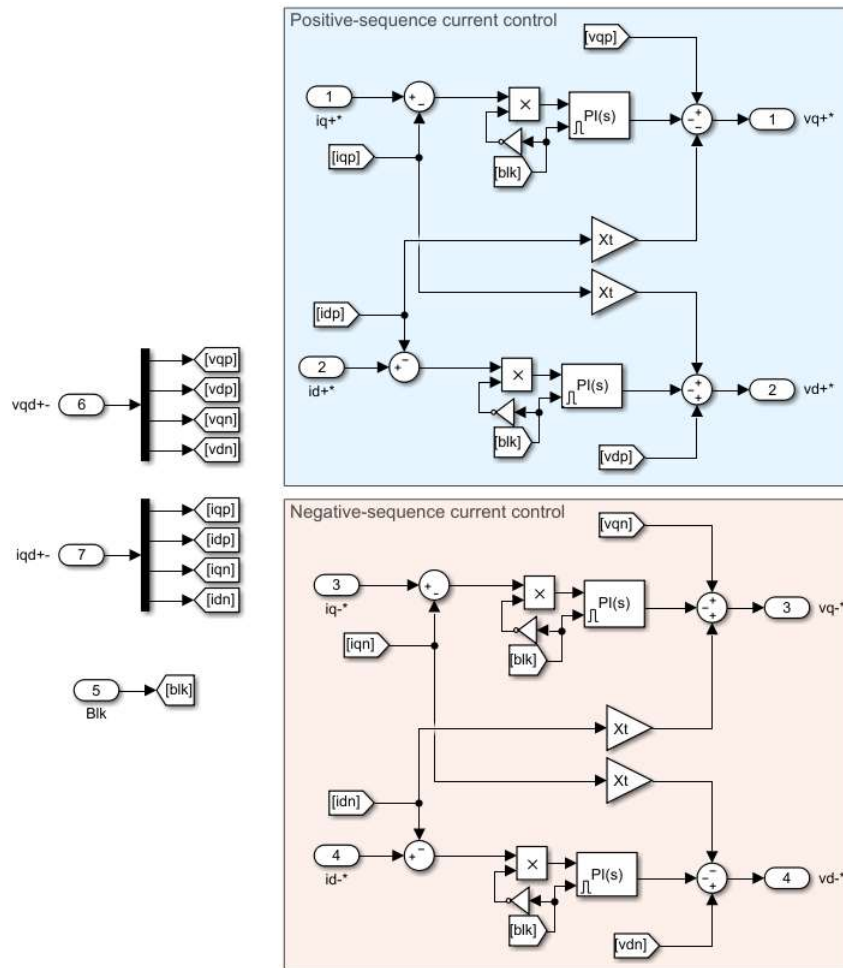


Figure 25 – Inner loop in the detailed control loops block.

2.4.2.2 Control loops – Phasor I-1st

In this model, the current-loop PI controller was substituted by a first order transfer function with time constant equal to the original current-loop time constant.

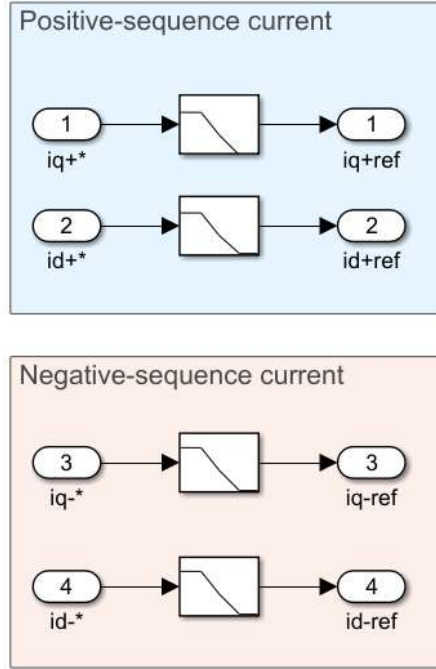


Figure 26 – Inner loop approximated by a first-order transfer function in the Phasor I-1st model.

2.4.2.3 Control loops – Phasor I-ref

In this model, the current loop is eliminated, thus neglecting its dynamics. It is assumed that the current reference is directly passed to the electrical part (controllable current source).

One difference in this model is that, as the current-loop dynamics are neglected, the PI controller parameters needed to be redesigned. The design goal was to have a power-loop time constant equal to the original power-loop time constant.

Thus, we want:

$$\frac{G_{pq}(s)}{1 + G_{pq}(s)} = \frac{1}{1 + \omega_{pq}s} \quad (8)$$

Where ω_{pq} is the original power loop bandwidth and $G_{pq}(s)$ is the new open-loop transfer function given by:

$$G_{pq}(s) = C_{pq} \frac{3}{2} v_q \quad (9)$$

Where C_{pq} is the new power-loop controller. Solving (1) for C_{pq} we have:

$$C_{pq}(s) = \frac{2}{3v_q} \omega_{pq} \frac{1}{s} \quad (10)$$

Thus, this PI controller was substituted by an integrator with gain equal to $\frac{2}{3v_q} \omega_{pq}$.

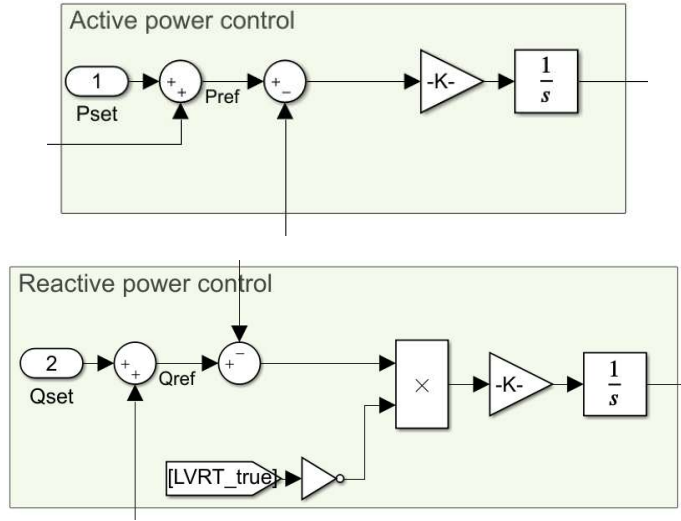


Figure 27 – Outer loop modified considering the elimination of the inner loop in the Phasor I-ref model.

2.4.2.4 Control loops – Phasor PQ-1st

In this model, the outer-loop PI controller was substituted by a low-pass filter with a time constant equal to the original closed-loop time constant. Thus, the current references were calculated using equation (11):

$$\begin{bmatrix} i_{qref} \\ i_{dref} \end{bmatrix} = \frac{2}{3v_q} \begin{bmatrix} P_{ref} \\ Q_{ref} \end{bmatrix} \quad (11)$$

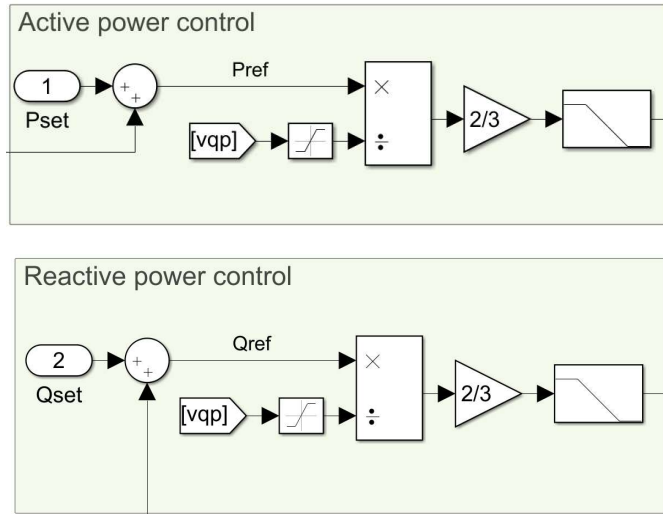


Figure 28 – Outer loop approximated by a first-order transfer function in the Phasor PQ-1st model.

2.4.3 Modulation block (dq to abc transformation)

The reference voltages are transformed from dq to abc in the Modulation block. Even though the modulation occurs only in the SW model, the same name was maintained for the other models. In this block, variant subsystems were also used to consider the differences among the models.

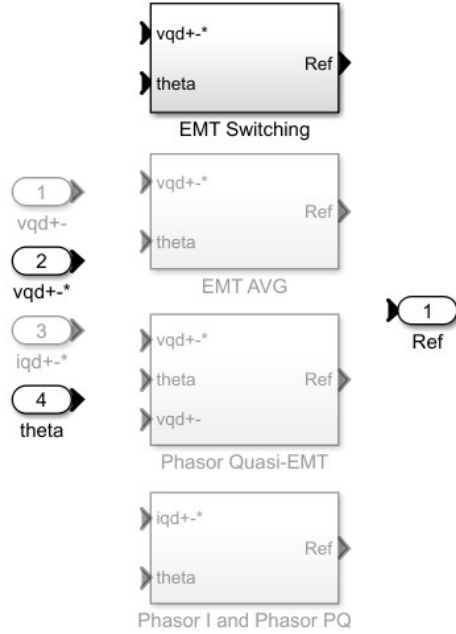


Figure 29 – Variant subsystems inside the Modulation block.

2.4.3.1 Modulation block – EMT SW

In the EMT SW model, the dq variables have first the delay corrected (filtering + simulation time step delay + transformer connection) and afterwards are transformed to the abc axis using the inverse Park transform. After the variables are transformed to the abc axis in both positive and negative sequences, they are summed and transformed in pulses for the IGBT bridge using SPWM. The PWM block is interpolated in time, which means that Simulink considers the exact time instant when the carrier crossed the modulated signal even when this happens between two simulation time steps. This increases the simulation precision.

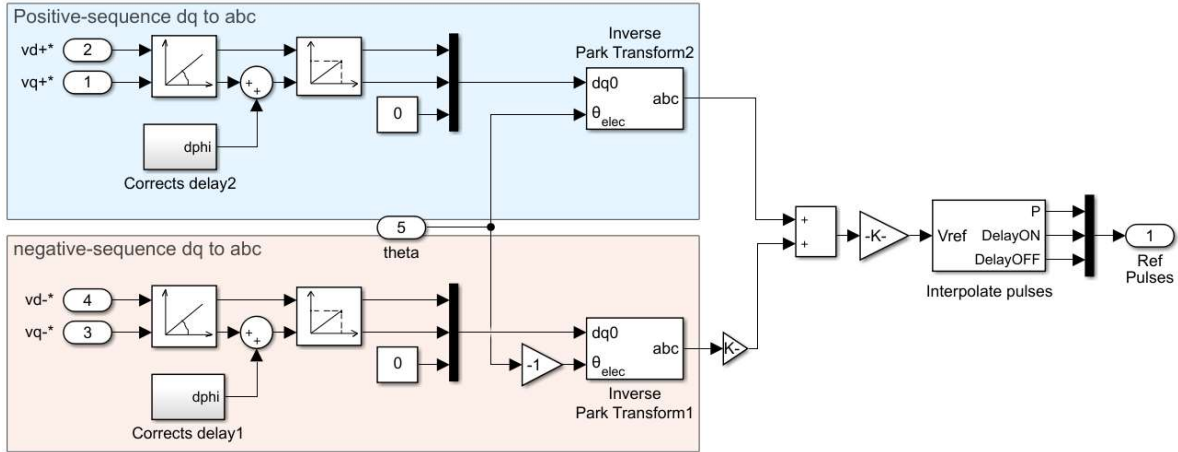


Figure 30 – SW model modulation.

2.4.3.2 Modulation block – EMT AVG

In the AVG model, there is no modulation. Thus, the calculated abc voltages are directly sent to the dependent voltage sources in the electrical part (Figure 31).

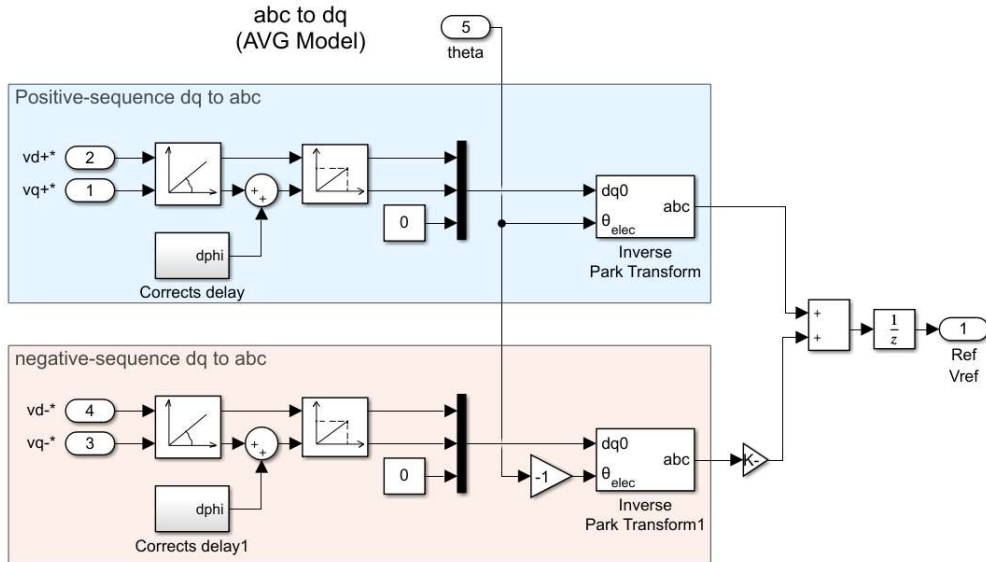


Figure 31 – AVG model dq to abc transformation.

2.4.3.3 Modulation block – Phasor QEMT

The Phasor models use the sequence to abc components transformation instead of the inverse park transform.

As phasor simulation considers steady-state condition, currents and voltages are calculated using only algebraic equations, without considering RL or RC time constants. Thus, to approximate the VSC Phasor model to the EMT models, the converter output voltage was transformed in a current signal considering the RL time constant of the transformer connected to the VSC. In this way, the signal sent to the

dependent current sources in the electrical part is the current that would flow through the RL element if the VSC voltage was applied in the time domain (Figure 33).

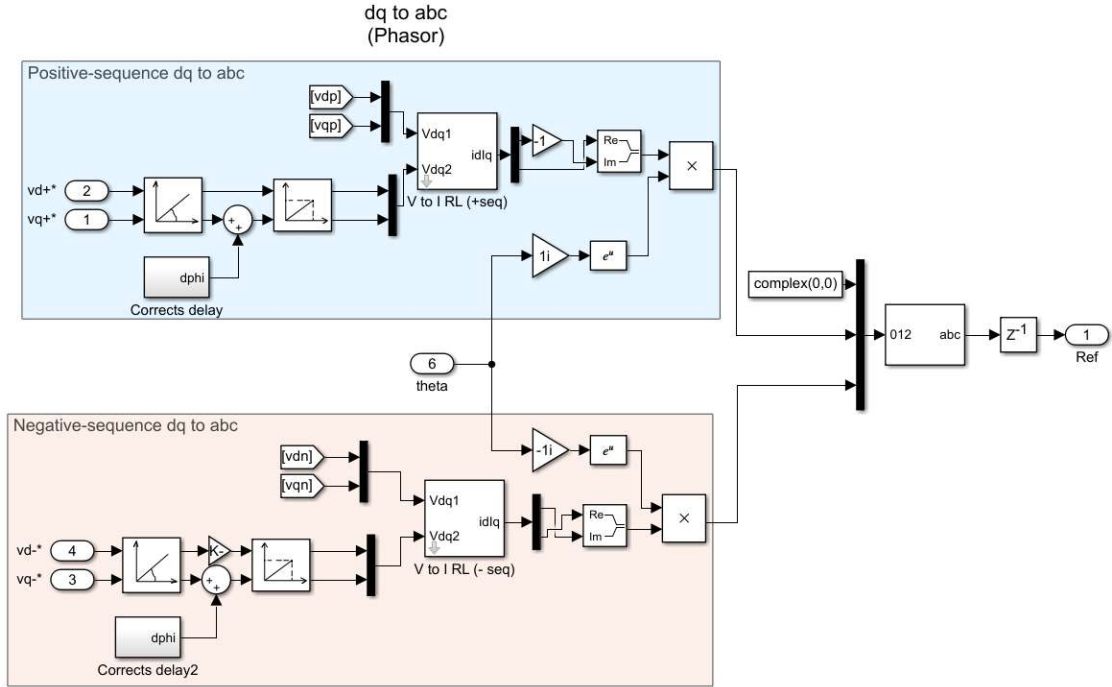


Figure 32 – Phasor QEMT model abc to dq transformation.

This subsystem converts the VSC output voltage in a current signal through an RL element

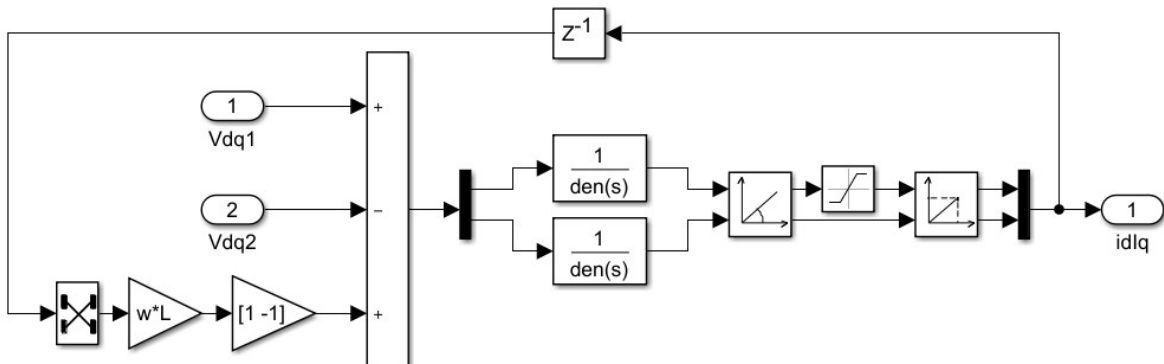


Figure 33 – Adding RL time constant to Phasor QEMT model output reference.

2.4.3.4 Modulation block – Phasor I-1st, Phasor I-ref and Phasor PQ-1st

In the other Phasor models, the electrical RL dynamics was neglected and the controllers' current references were transformed directly to the abc axis.

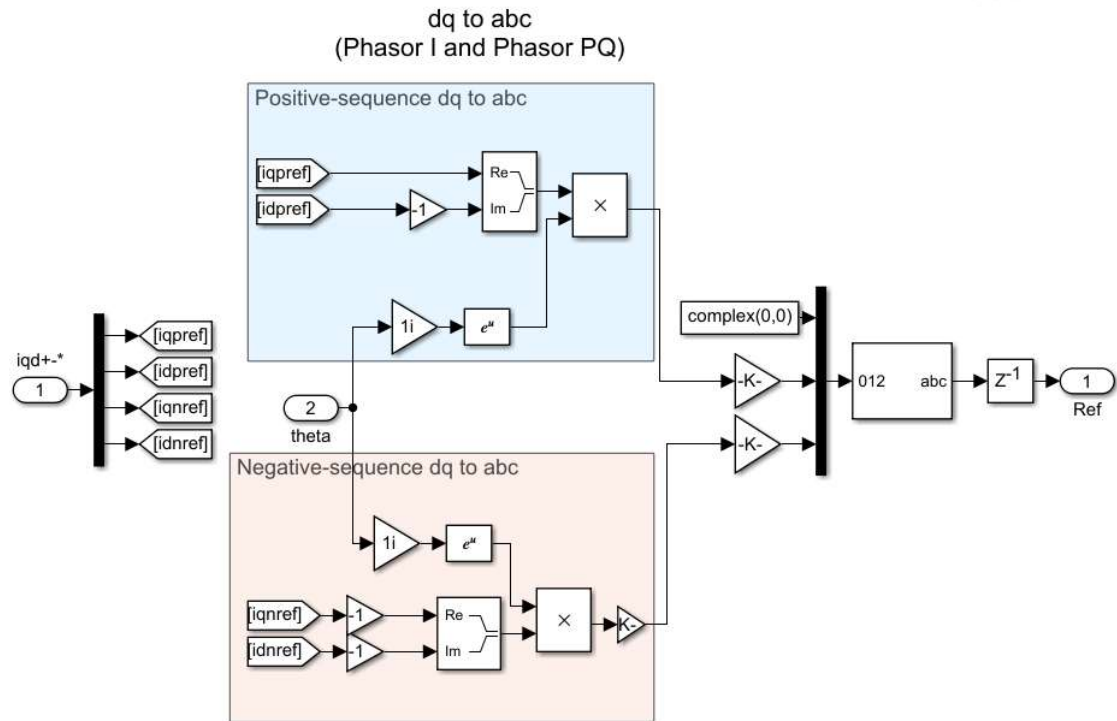


Figure 34 – Phasor I-1st ,I-ref and PQ-1st Modulation block.

3 Synchronous generator model

Synchronous generators (SGs) play a key role in overall system stability. Thus, although the focus of the study was the VSC, the SGs were also modelled, in order to study their interaction with the VSC. Well-known SG models were used, which provided the required precision for the studies while keeping a desirable simplicity.

3.1 Electrical model

The SGs were modelled using the Model 2.2 of [10], a precise yet simple electrical model in the dq axis. This model takes into account the dynamics of the stator, field, and damper windings. One of the benefits of this model is that standard data supplied by manufacturers is usually based on this model structure [11]. In this study, no saturation was considered. The equivalent circuit of the model is represented in the rotor reference frame (dq frame). Stator windings are connected in wye to an internal neutral point.

The model equivalent circuits in the d and q axis are shown in Figure 35 and Figure 36, respectively. The model variables are described in the Nomenclature.

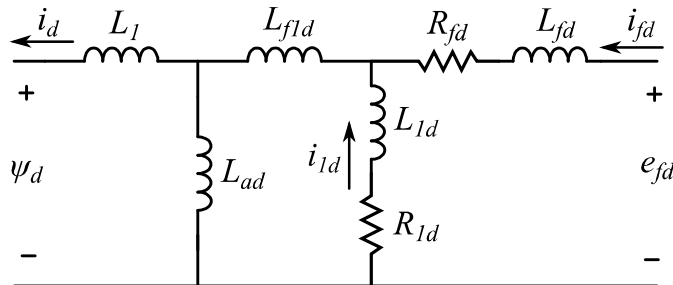


Figure 35 – SG model d-axis equivalent circuit [10].

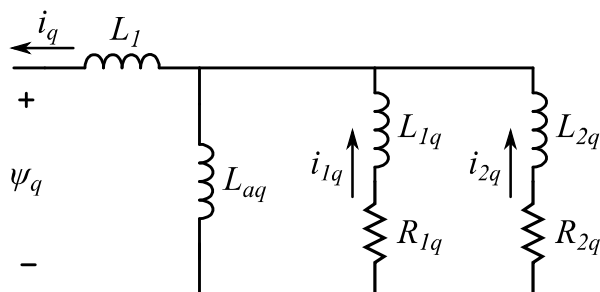


Figure 36 – SG model q-axis equivalent circuit [10].

The SG voltages are calculated as:

$$\begin{bmatrix} v_d \\ v_q \\ v_0 \\ v_{fd} \end{bmatrix} = -\begin{bmatrix} i_d R_a \\ i_q R_a \\ i_0 R_0 \\ i_{fd} R_{fd} \end{bmatrix} - \omega \begin{bmatrix} \psi_q \\ \psi_d \\ 0 \\ 0 \end{bmatrix} + \begin{bmatrix} \frac{d\psi_d}{dt} \\ \frac{d\psi_q}{dt} \\ \frac{d\psi_0}{dt} \\ \frac{d\psi_{fd}}{dt} \end{bmatrix} \quad (12)$$

Where ω is the SG speed in p.u., R_a is the SG armature resistance, R_0 is the zero-sequence resistance and R_{fd} is the field circuit resistance. The fluxes in (12) are calculated as

$$\begin{bmatrix} \psi_d \\ \psi_{1d} \\ \psi_{fd} \end{bmatrix} = \frac{2}{3} \begin{bmatrix} L_{ad} + L_1 & L_{ad} & L_{ad} \\ L_{ad} & L_{1d} + L_{f1d} + L_{ad} & L_{f1d} + L_{ad} \\ L_{ad} & L_{f1d} + L_{ad} & L_{fd} + L_{f1d} + L_{ad} \end{bmatrix} \begin{bmatrix} -i_d \\ i_{1d} \\ i_{fd} \end{bmatrix} \quad (13)$$

$$\begin{bmatrix} \psi_q \\ \psi_{1q} \\ \psi_{2q} \end{bmatrix} = \begin{bmatrix} L_{aq} + L_1 & L_{aq} & L_{aq} \\ L_{aq} & L_{aq} + L_{1q} & L_{aq} \\ L_{aq} & L_{aq} & L_{aq} + L_{2q} \end{bmatrix} \begin{bmatrix} -i_q \\ i_{1q} \\ i_{2q} \end{bmatrix} \quad (14)$$

And the electromechanical torque (T_e) is given by:

$$T_e = \frac{3}{2} \left(\frac{N_p}{2} \right) (\psi_d i_q - \psi_q i_d) \quad (15)$$

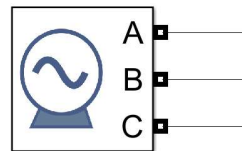
Where N_p is the number of poles of the SG. The damper windings voltages are equal to zero because they are internally shorted windings. A more in-depth description of this model can be found in [10].

As the SG is modelled as a current source in Simulink, a snubber was connected to the SGs terminals to avoid numerical oscillations. The snubber was a resistive load equal to 5% of the SGs nominal power.

3.2 Control system

As the focus of this study was on the VSC, the SGs were simulated using simple models for the speed governor, exciter and Power System Stabilizer (PSS).

The SG model in Simulink is depicted in Figure 37. Internally, the model is composed of the SG electromechanical model (G1 in Figure 38), the speed governor (Figure 39) and the exciter system (Figure 40).



Synchronous machine

Figure 37 – Modelled SG in Simulink.

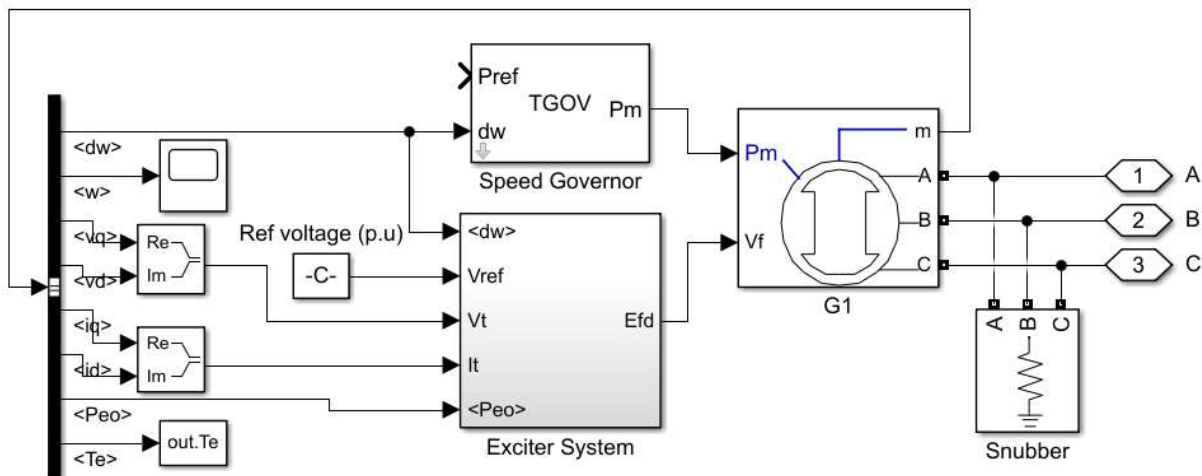


Figure 38 – Subsystems that compose the SG model.

3.2.1 Speed governor model

The speed governor model was inspired on the simple TGOV1 model [12]. It is the simplest speed governor mode, comprising droop, one time constant for the valve and one lead/lag block to represent the turbine. The only difference between the modelled speed governor and the TGOV1 is that in TGOV1 the droop constant $1/R$ multiplies the sum ($RefL - dw$), while in the implemented model it multiplies dw only. This in practice only changes the scale of the $RefL$ and has no other influence on the SG model. The model nomenclature can be found in [12].

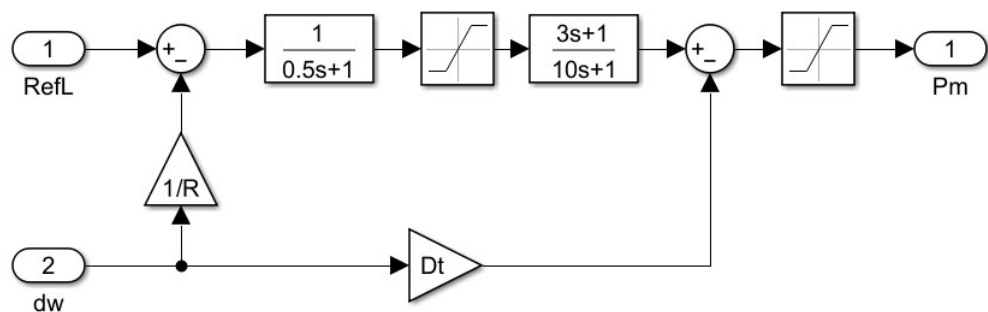


Figure 39 – Speed governor model.

3.2.2 Exciter system model

The exciter system model (Figure 40) was composed of the transducer and load compensation (Figure 41), PSS (Figure 42) and exciter models (Figure 43). The goal of the exciter system is to define the required field voltage (E_{fd} in Figure 40) to produce the defined voltage at the SG terminals. The structure of the exciter system, as well as its subsystems, were based on [13].

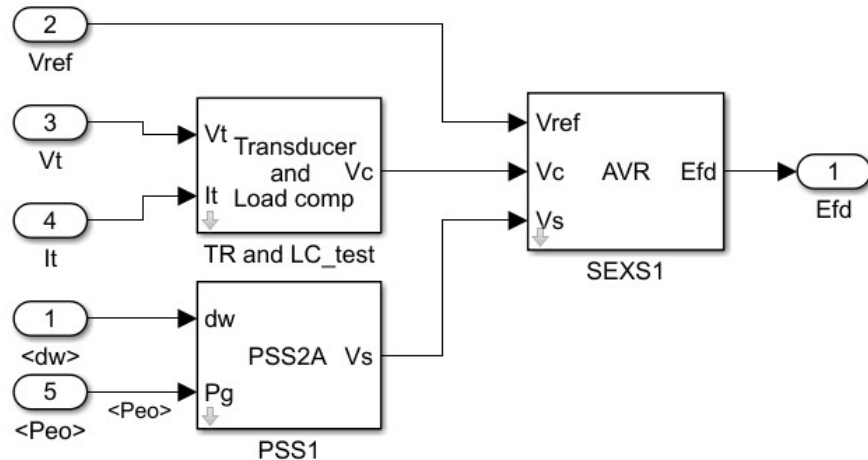


Figure 40 – Exciter system model.

If the voltage setpoint is required to be controlled after a line, transformer or other element connected to the SG, the element's impedance can be compensated in the voltage regulation. In this study, the voltage was controlled at the SG terminals, thus no impedance compensation was performed. Moreover, a very simple transducer model was used, represented by a first-order transfer function with a time constant equal to 1 ms.

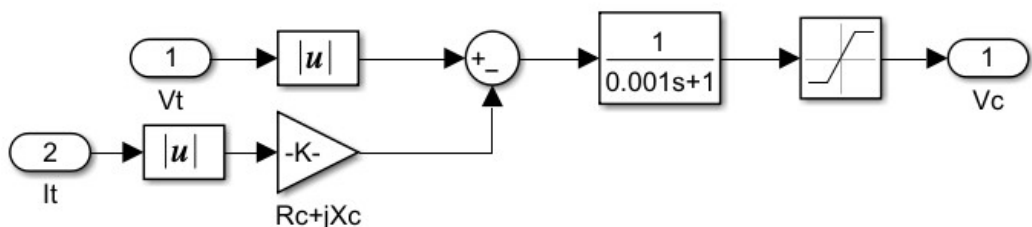


Figure 41 – Transducer and load compensation model.

The PSS model was based on the PSS2A model, described in [13].

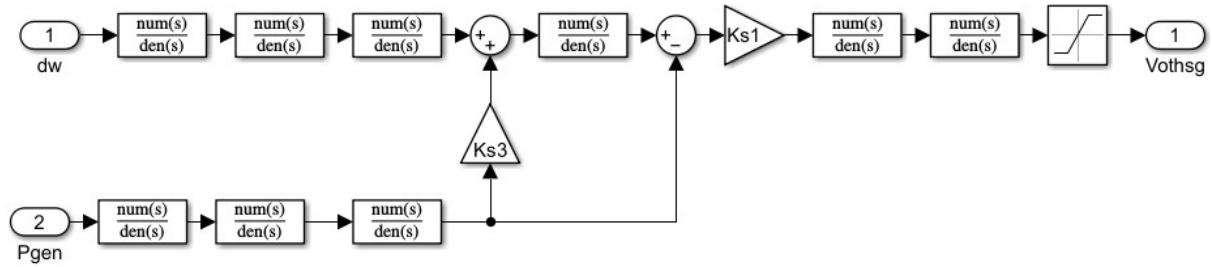


Figure 42 – PSS model.

The exciter was modelled using the Simplified Exciter System Model (SEXS), the same as used in [14], similar to the model AC4A in [13].

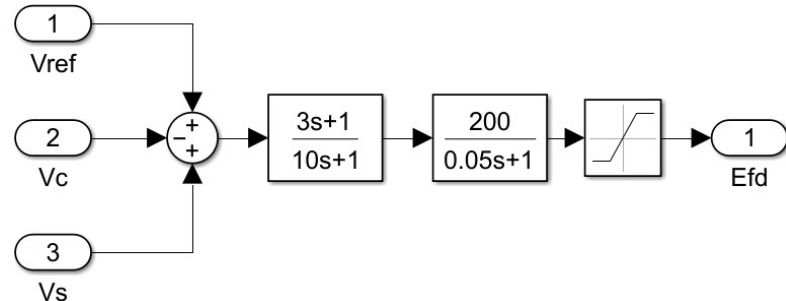


Figure 43 – Exciter model.

4 Case studies – VSC model

In this section, a list of simulated case studies using the developed VSC models is discussed. The tests were:

1. **Setpoint tracking**
 - o **PLL**
 - o **Current-controller**
 - o **Power-controller**
2. **Load and generation variations**
 - o **Load change**
 - o **Voltage variation**
 - o **Frequency variation**
3. **Frequency droop**
4. **Voltage droop**
5. **Symmetrical fault + LVRT**
6. **Asymmetrical fault + negative sequence control**

The majority of the tests were simulated in the test system depicted in Figure 44. When a test was conducted in a different system, it has been indicated.

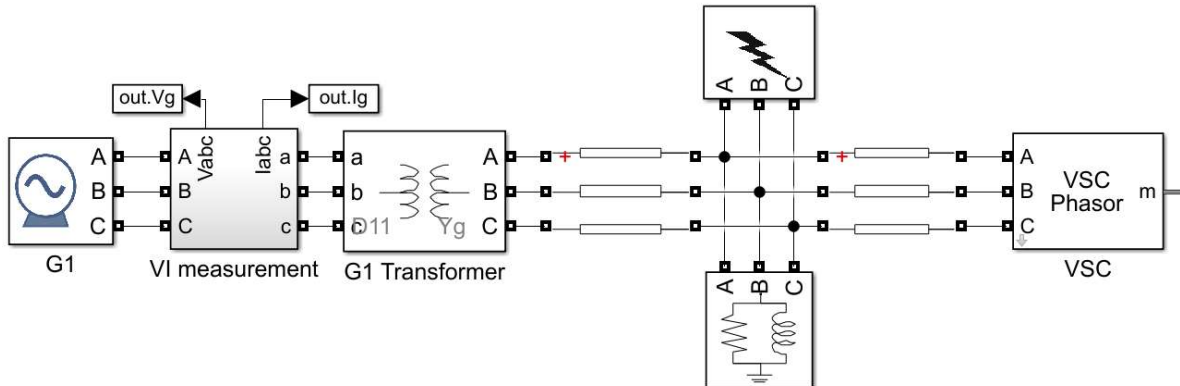


Figure 44 – Simulated system.

Where G1 is a 500 MVA salient-pole synchronous generator modelled according to [14] (Figure 45).

Synchronous Machine Model according to ENTSO-E

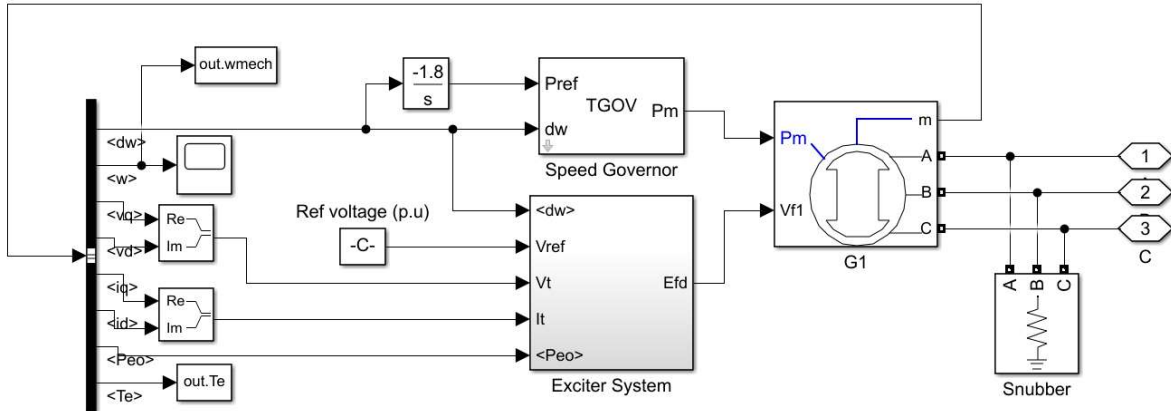


Figure 45 – Modelled synchronous generator.

As the test system has only one synchronous generator, it was controlled in isochronous mode.

4.1 Setpoint tracking

The aim of this test was to verify if the control loops were behaving as designed. Thus, to remove the influence of external elements, the VSC was directly connected to an ideal voltage source.

4.1.1 PLL

The PLL was designed to have a $2\pi 80$ bandwidth that results in a settling time of 12.5 ms. This settling time can be observed in Figure 46, during the PLL initialization.

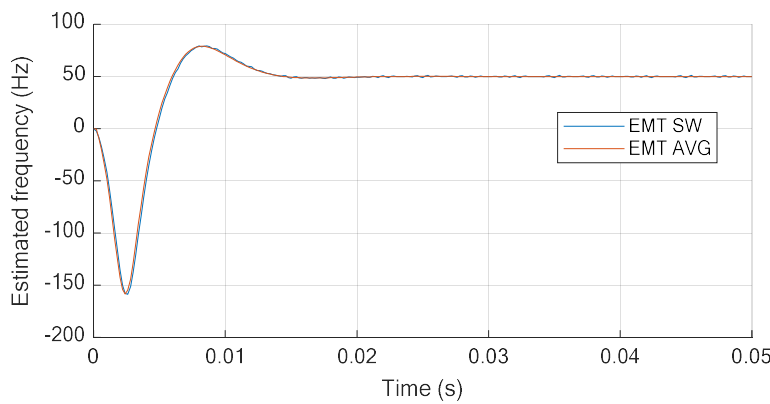


Figure 46 – PLL initialization.

4.1.2 Current-controller

The current controller was designed to have bandwidth of $2\pi 135$ rad/s, resulting in a rising time of 2.59 ms. It can be observed from Figure 47 that in all models (SW, AVG and Phasor) the setpoint was tracked correctly and within the designed rising time.

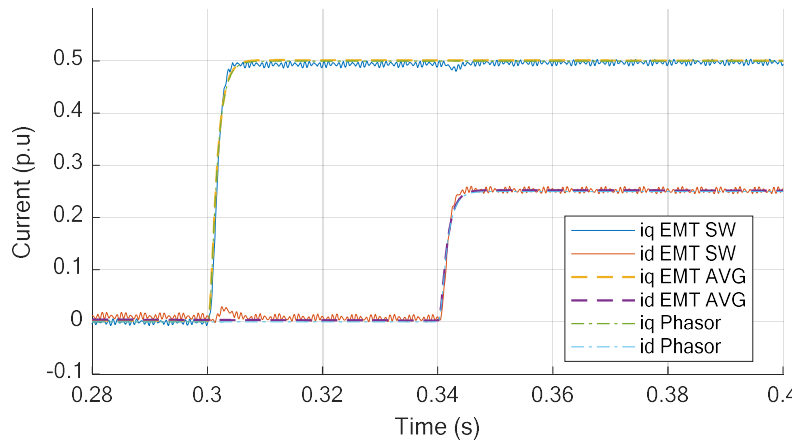


Figure 47 – Output-current setpoint tracking.

4.1.3 Power-controller

The current controller was designed to be 10 times slower than the output-current loop, with rising time of 25.9 ms. It can be observed from Figure 48 and Figure 49 that in all models (SW, AVG and Phasor) the setpoint was tracked correctly and within the designed rising time.

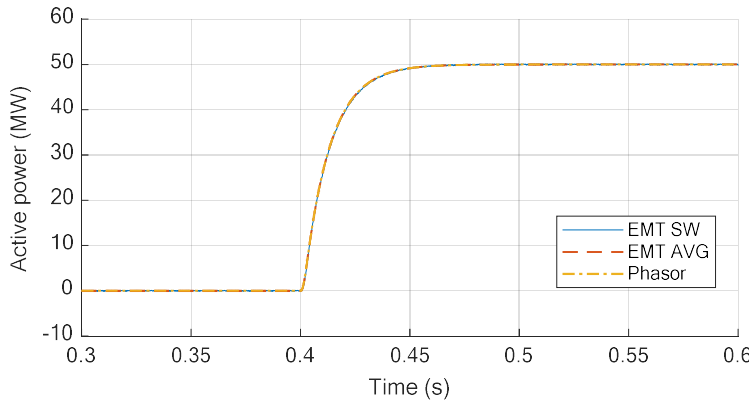


Figure 48 – Active power setpoint tracking.

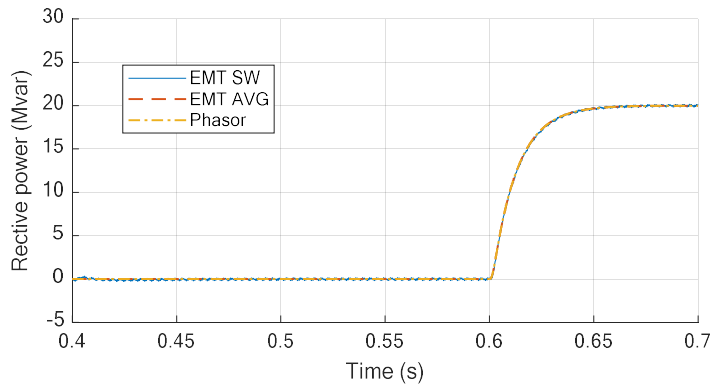


Figure 49 – Reactive power setpoint tracking.

4.2 Load and generation variations

The next test was to vary load and generation conditions in the system of Figure 44. During these tests, voltage and frequency drops were disabled.

4.2.1 Load change

The system of Figure 44 was initialized with a load of 47.5 MW, 7.6 Mvar. At $t = 0.4$ s and $t = 0.6$ s, the active and reactive powers were set to -30 MW and -10 Mvar, respectively. At $t = 1.0$ s, the load was doubled to 95 MW and 15.2 Mvar. The results are depicted in Figure 50. As can be observed, in the three models the converter kept the power setpoints even during a load variation.

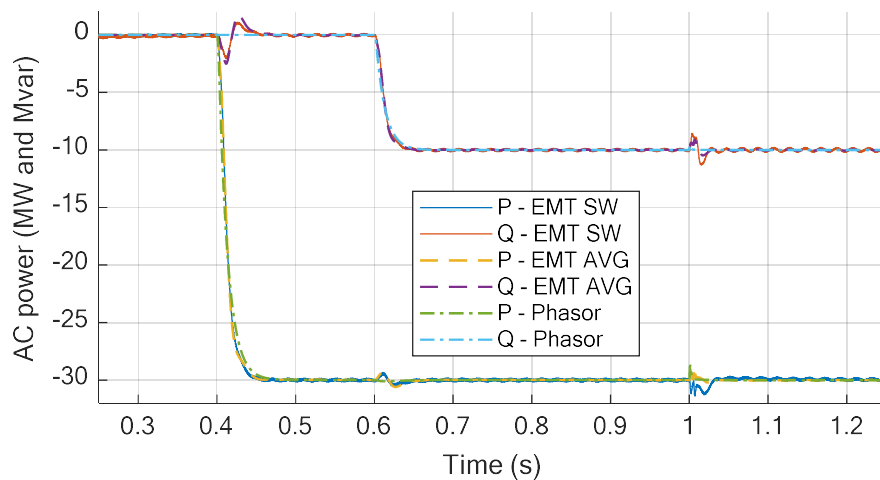


Figure 50 – Converter AC power during load change.

4.2.2 Voltage variation

For this test, the generator voltage reference was changed from 1 p.u to 0.9 p.u at $t = 1$ s. The converter power setpoint was defined as the same of the previous test. As can be observed, the voltage variation had no influence on the converter output power.

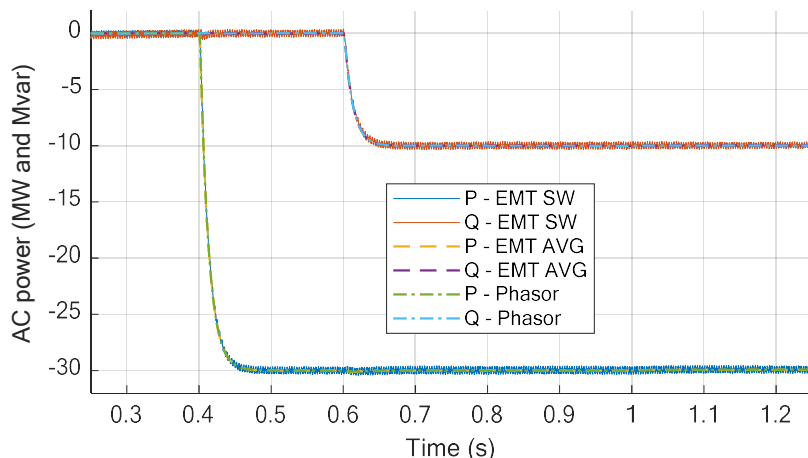


Figure 51 – Converter AC power during a voltage variation.

4.2.3 Frequency variation

In this test, a 200 MW, 40 Mvar load is connected to the system at $t = 0$ s, which causes the generator frequency to drop, as depicted in Figure 52.

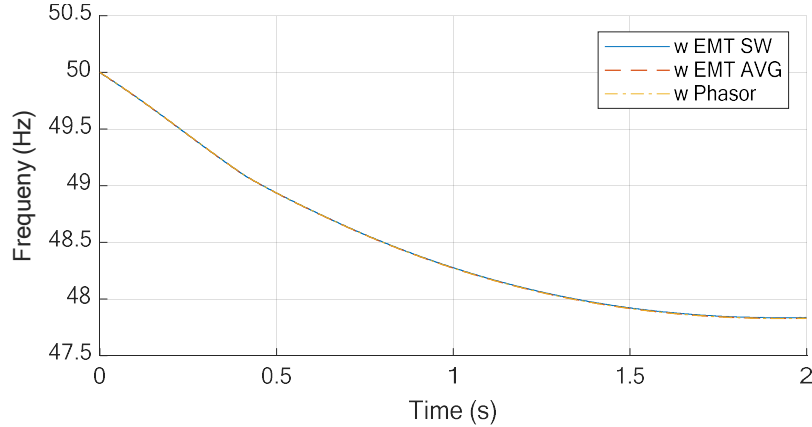


Figure 52 – Generator speed during a sudden load increase.

The converter output power is depicted in Figure 53. As can be observed, the frequency variation had no influence on the converter output power.

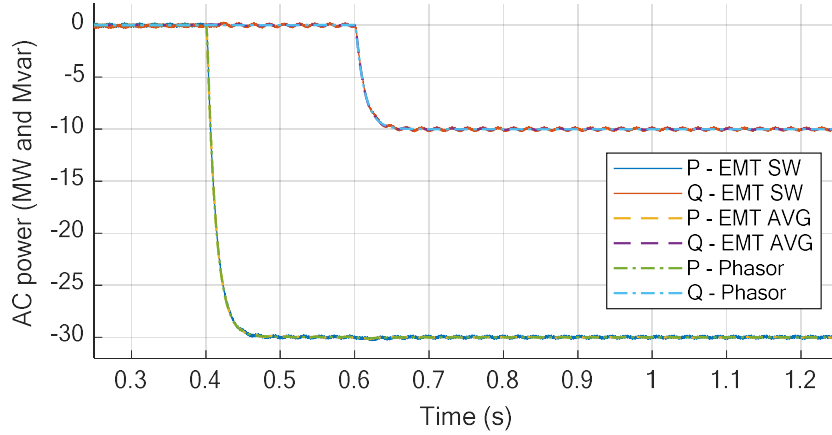


Figure 53 – Converter power during a frequency variation.

4.3 Frequency droop

In this test, the converter frequency droop was enabled. Also, both active and reactive powers were set to zero to facilitate the visualization of the converter contribution to restore the frequency.

At $t = 0$ s, a 47.5 MW, 7.6 Mvar load is connected to the system which causes the generator frequency to drop (Figure 54). The VSC droop was set to 10% and the converter was limited to participate in the frequency regulation up to 10% of its power. The converter output power is depicted in Figure 55. As can be observed in the figures,

the converter injects active power to restore the frequency to 50 Hz. Moreover, the power injected and the frequency is nearly the same in the three models.

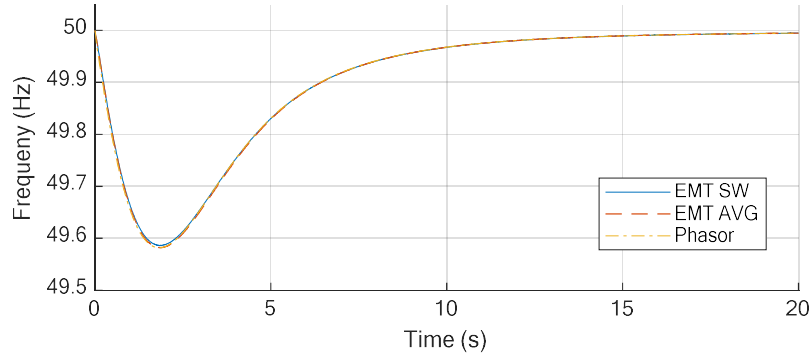


Figure 54 – Frequency during a load increase with VSC droop.

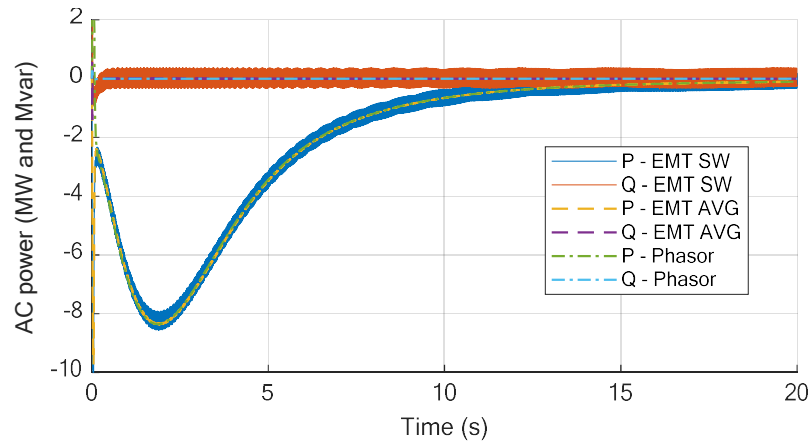


Figure 55 – Converter output power during a frequency variation.

4.4 Voltage droop

In this test, the converter voltage droop was enabled and both active and reactive powers were set to zero. At $t = 1.0$ s, the generator voltage setpoint was changed from 1.01 p.u to 0.91 p.u and at $t = 3.0$ s, the voltage setpoint was restored to 1.01 p.u (Figure 56). The converter output power is depicted in Figure 57. It can be observed that the converter has injected reactive power proportional to the voltage deviation. When the voltage was higher than 1 p.u, the converter absorbed reactive power. When the voltage was lower than 1 p.u, the converter provided reactive power.

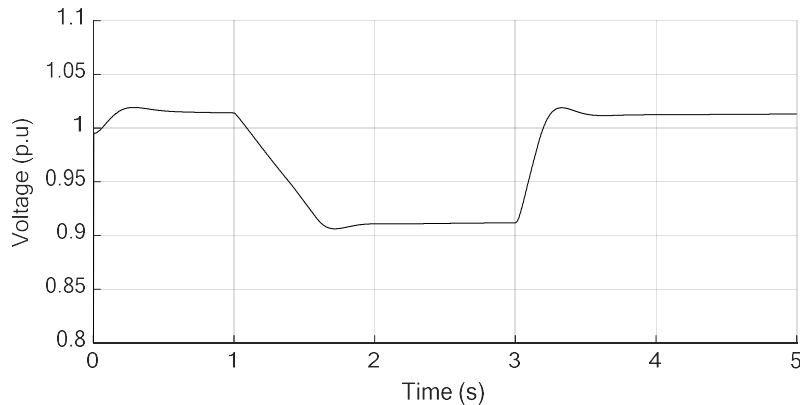


Figure 56 – AC voltage during voltage droop test.

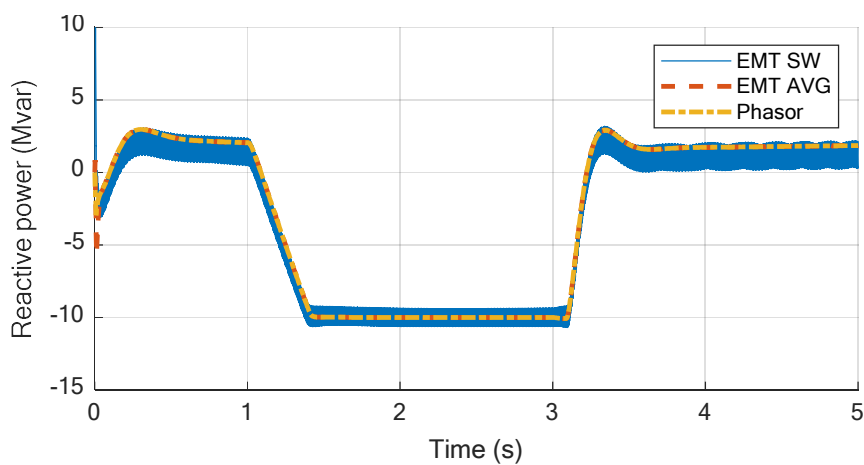


Figure 57 – Converter output reactive power during voltage droop test.

4.5 Symmetrical fault + LVRT

In this test, a 10Ω three-phase fault is applied in the point between the transmission lines that connect the VSC to the synchronous machine. The fault is applied between $t = 0.5$ and after 300 ms it was cleared.

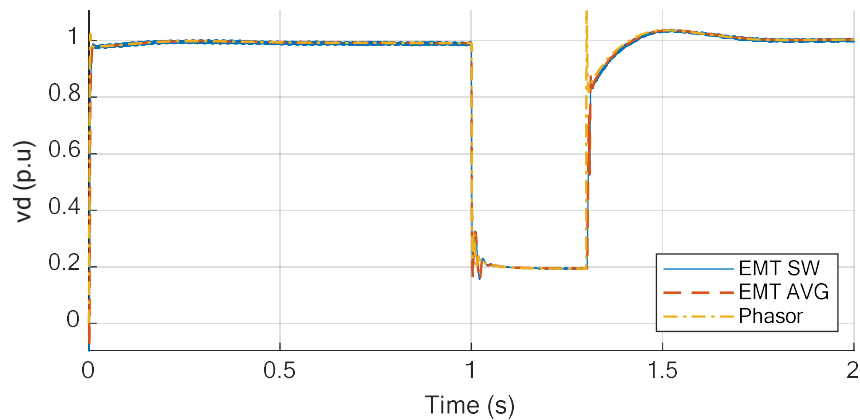


Figure 58 – AC voltage magnitude during the three-phase fault.

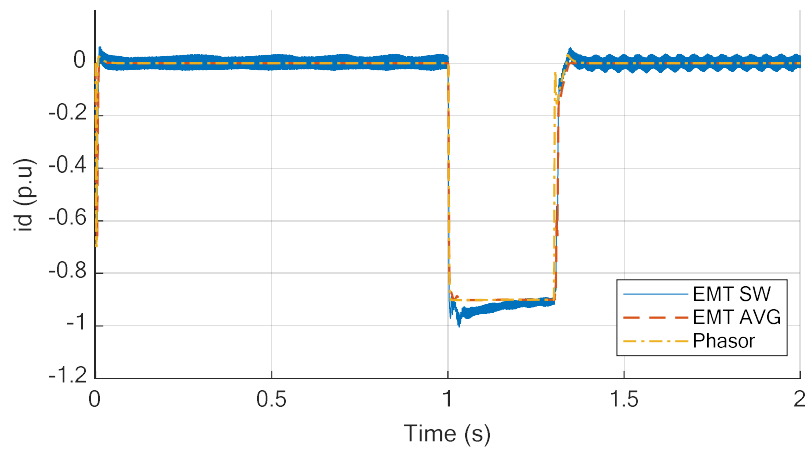


Figure 59 – Reactive current injection provided by the LVRT.

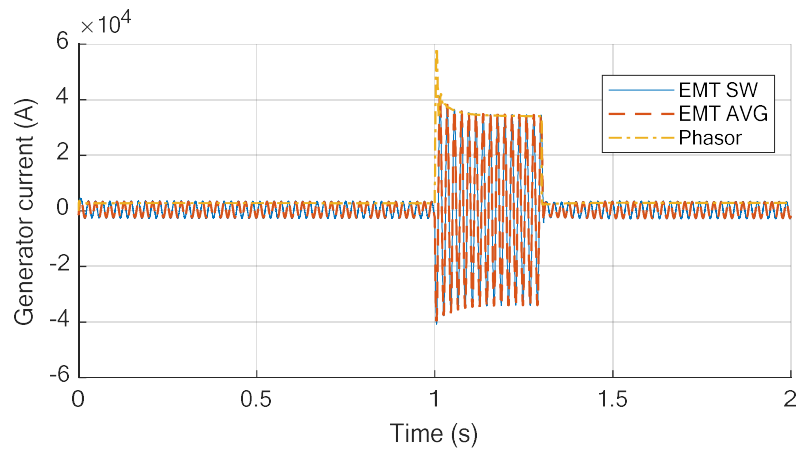


Figure 60 – Generator current during the three-phase fault.

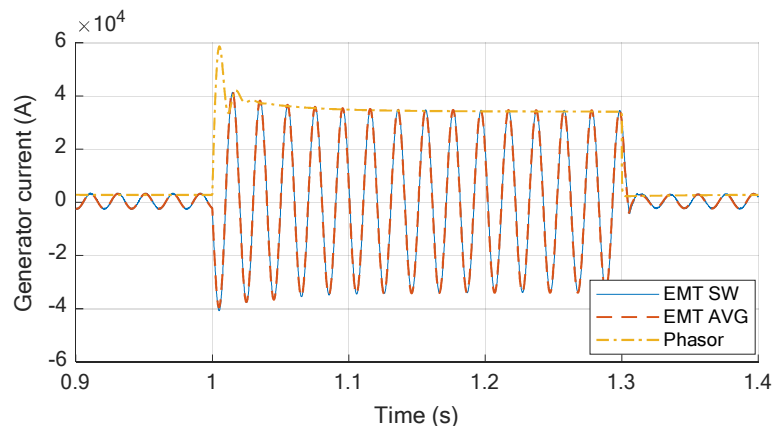


Figure 61 – Generator current during the three-phase fault, detail on the first instants of the fault.

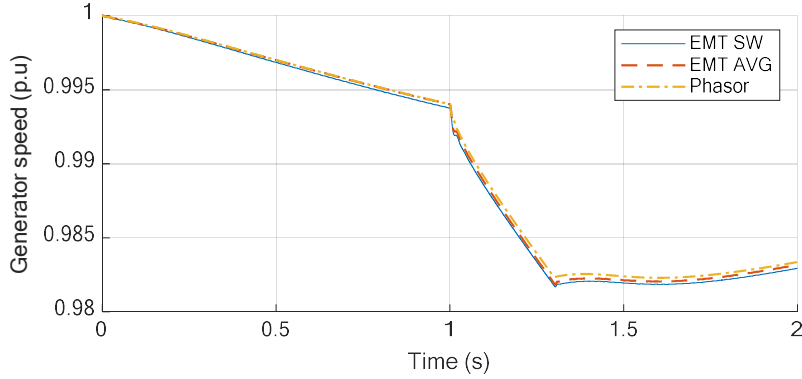


Figure 62 – Generator speed during the fault.

From the present results it is possible to observe a very good agreement among the three models, even during an extreme event as a symmetrical fault. Slight differences are: In Figure 59 the SW model takes 200 ms to follow the current reference defined by the LVRT, which can be explained by the converter modulation limitations during low voltage conditions. And, second, in Figure 61 the generator current in the Phasor model takes 20 ms to match the EMT models. In general, an excellent matching was observed among the three models.

4.6 Asymmetrical fault + negative sequence control

In this test, an 8Ω mono-phase fault is applied in the Phase A of the point between the transmission lines that connect the VSC to the synchronous machine. The fault is applied between $t = 0.5$ and it was cleared after 300 ms. The results are presented in Figure

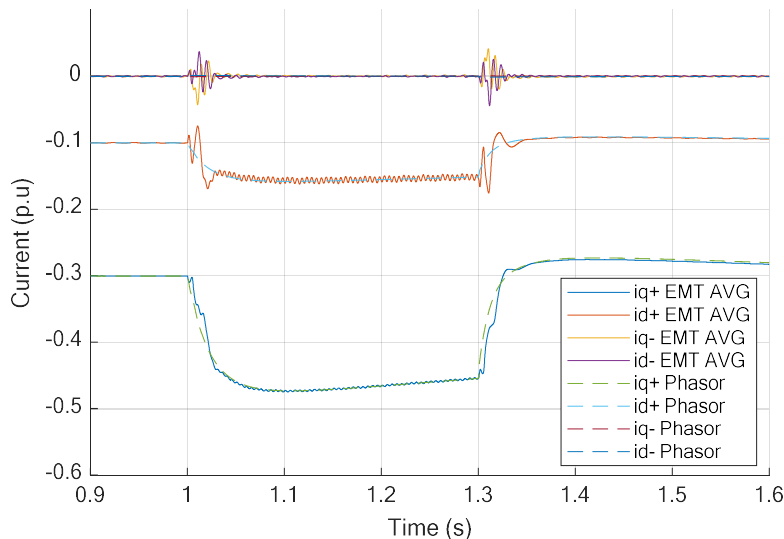


Figure 63 – Converter positive and negative sequence dq currents during the asymmetrical fault.

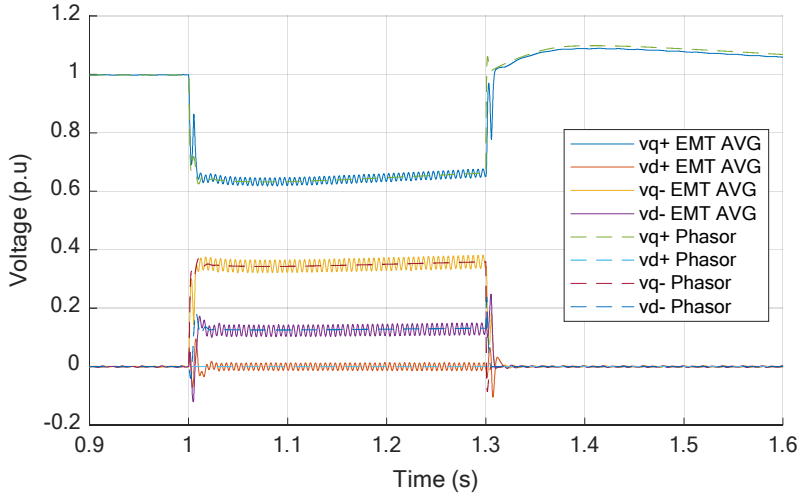


Figure 64 – Converter positive and negative sequence dq voltages during the asymmetrical fault.

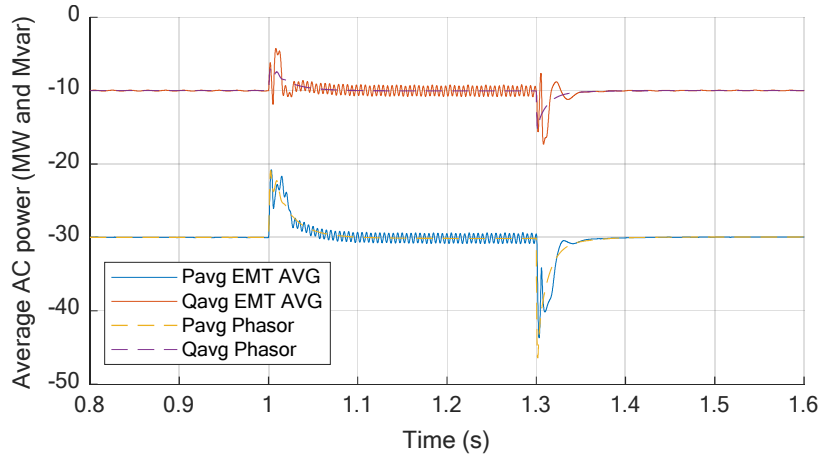


Figure 65 – Converter average AC power output during the asymmetrical fault.

From the results it is possible to observe a good agreement between EMT and Phasor models even during an asymmetrical fault. Slightly differences are observed during the beginning and the end of the transient, but they disappear after 40 ms (2 cycles).

4.7 Discussion

By observing the results of this section, the three models (SW, AVG and Phasor) presented very similar results for the majority of the cases tested. However, extreme conditions as the one analysed in section 4.5 review a key difference between EMT and Phasor models, which is the capacity to represent fast changes in the system. Phasor models present good precision for slow dynamics (< 10 Hz). However, for fast dynamics as short-circuits, some components are not represented adequately (e.g synchronous generator fault current contribution). Even tough, in these transient cases, after a few cycles, the response of the phasor models matches the response of the EMT models adequately.

5 Case studies – HV system

The Cigré-inspired HV network diagram is presented in Figure 66.

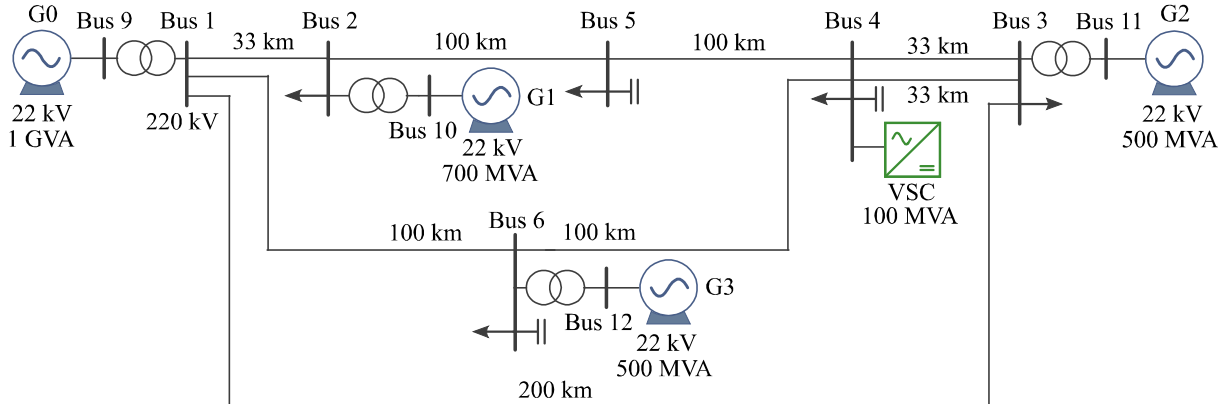


Figure 66 – Test system diagram.

The differences between the modelled test system and the original Cigré HV system were:

1. ***The infinite slack bus connected to bus 9 was substituted by an 1 GVA synchronous machine.***
2. ***The lines lengths were reduced by a third of their original values.***
3. ***The 380 kV circuit connecting Bus 1 to Bus 3 was transformed to a 220 kV circuit and the 220/380 kV transformers were removed.***
 - o ***The parameters of the line connecting Bus 1 to Bus 3 were based on the 220 kV configuration.***
4. ***Although buses 6b, 7 and 8 were removed, the same numbering was used for the other buses.***

A list of simulated case studies using the modelled HV system and the developed VSC models is discussed. The tests were:

- o ***Load variations***
- o ***Loss of generation***
- o ***Symmetrical fault***
- o ***Asymmetrical fault***
- o ***Line outage***

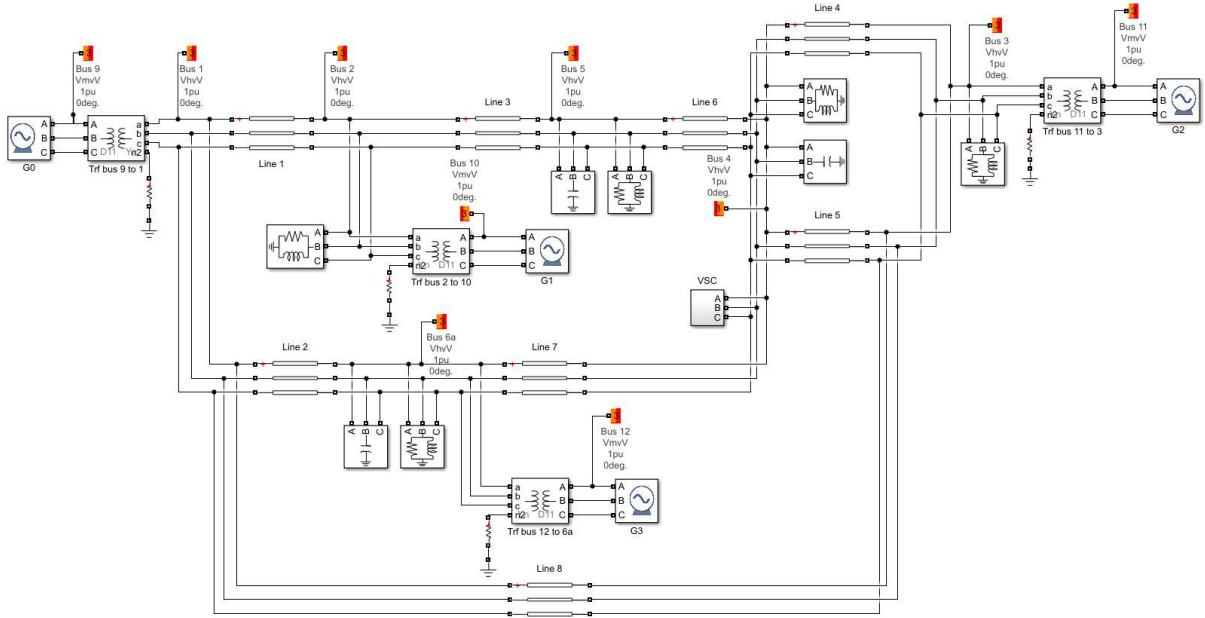


Figure 67 – HV test system modelled in Simulink.

A 100 MVA VSC was connected to bus 4. The VSC power setpoints were -30 MW, -10 Mvar. According to the convention used in this study, the VSC is absorbing power. Thus, negative power means that the VSC is providing active and reactive power to the system.

Frequency droop, voltage droop, LVRT and negative sequence control were enabled during all tests.

5.1 Load variation

The first test was to connect a 100 MW, 10 Mvar load to bus 5 at $t = 5$ s.

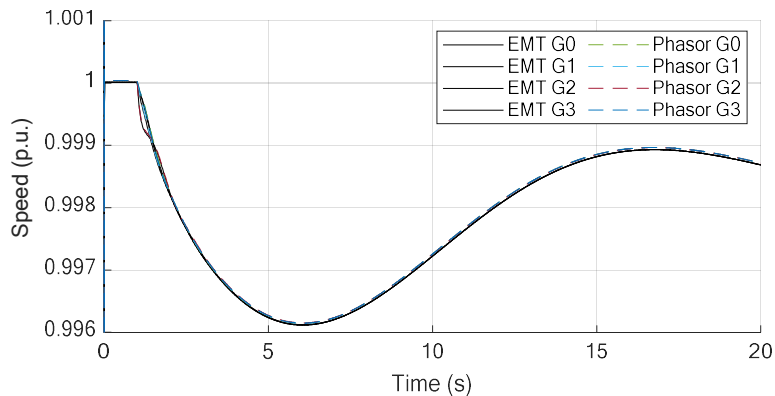


Figure 68 - SMs speeds during a load connection. VSC connected.

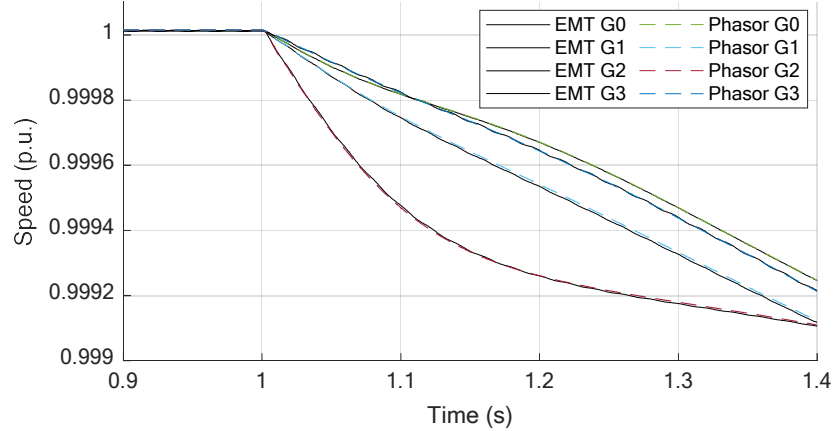


Figure 69 - SMs speeds during a load connection (detail). VSC connected.

From the results presented, an excellent agreement could be seen between Phasor and EMT models during the low-frequency transient produced by the load connection.

5.2 Loss of generation

In this test, the generator G1 was removed from the system at $t = 5$ s. The results are presented below.

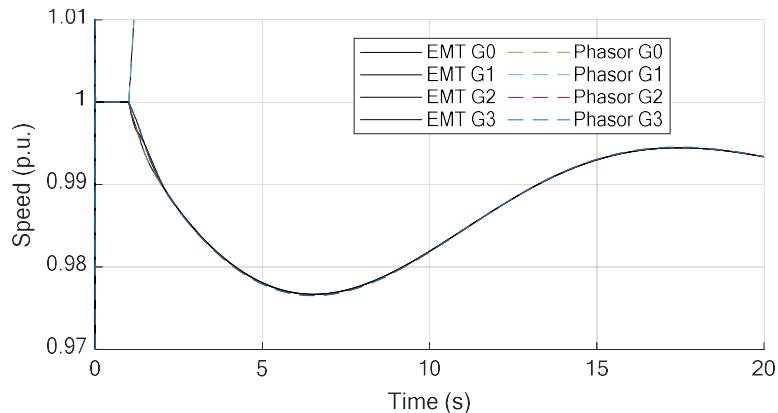


Figure 70 – SMs speeds during outage of G1. VSC connected.

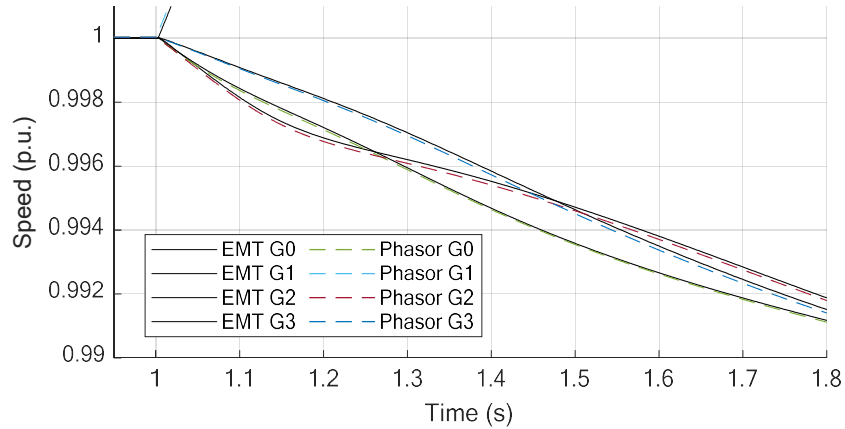


Figure 71 – SMs speeds during outage of G1 (detail). VSC connected.

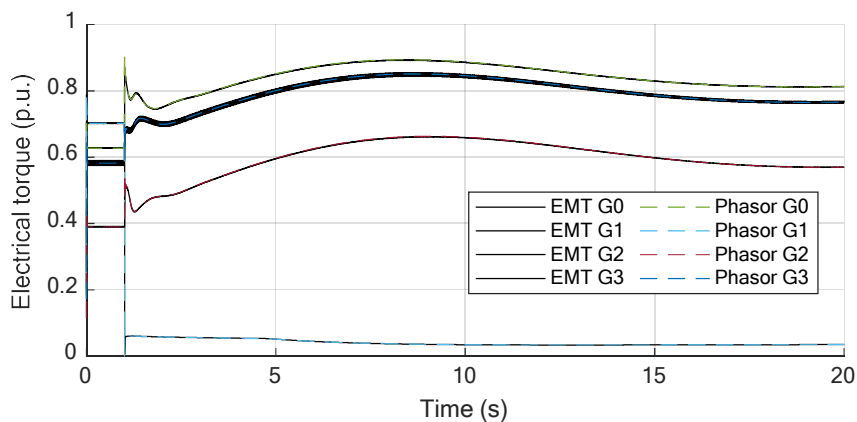


Figure 72 – SMs torques during outage of G1. VSC connected.

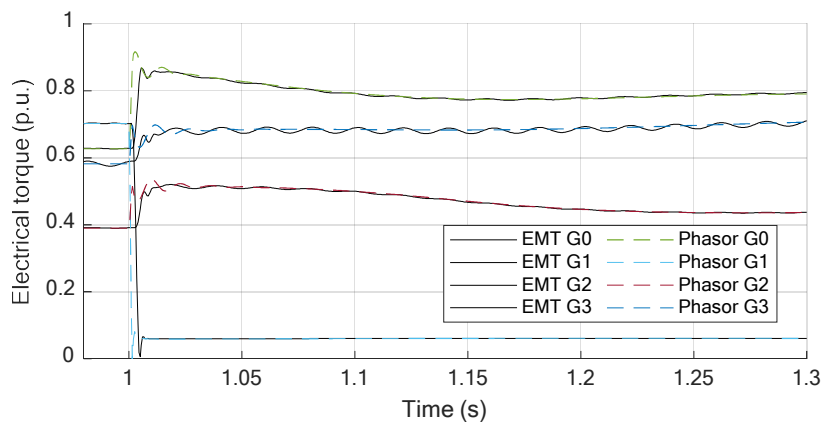


Figure 73 – SMs torques during outage of G1 (detail). VSC connected.

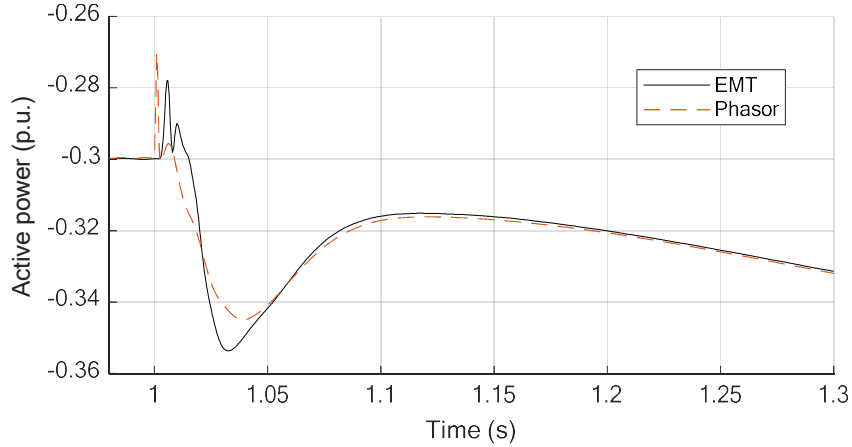


Figure 74 – VSC output AC power during outage of G1 (detail). VSC connected.

As well as in the other cases, the Phasor model presented similar results to the EMT model after 200 ms of the beginning of the transient.

5.3 Symmetrical fault

In this test, a temporary $10\ \Omega$ three-phase fault was applied at Bus 2 at $t = 1\text{ s}$. The results are shown below.

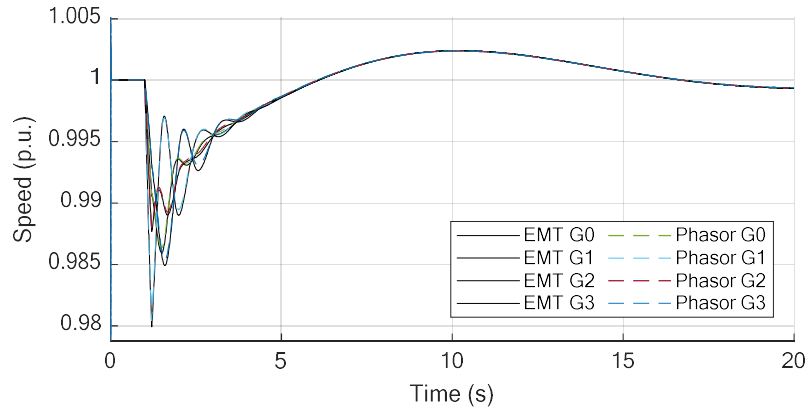


Figure 75 - SMs speeds during an symmetrical fault. VSC connected.

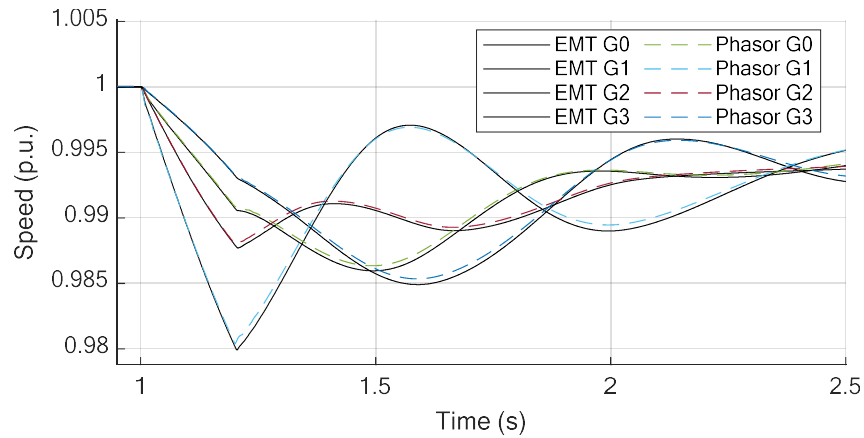


Figure 76 - SMs speeds during an symmetrical fault (detail). VSC connected.

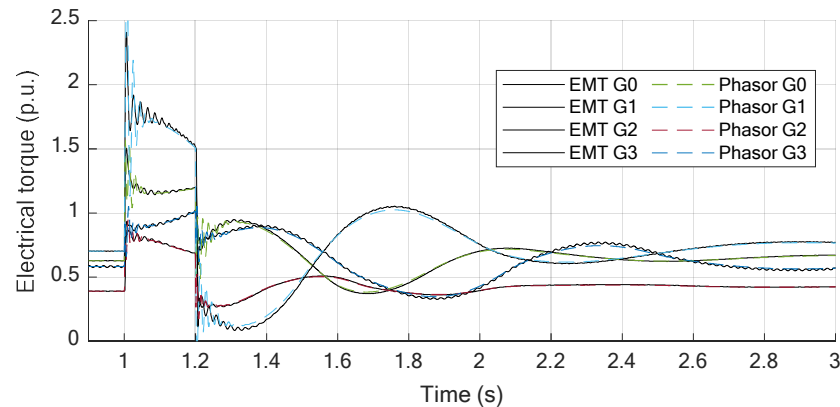


Figure 77 - SMs torques during an symmetrical fault (detail). VSC connected.

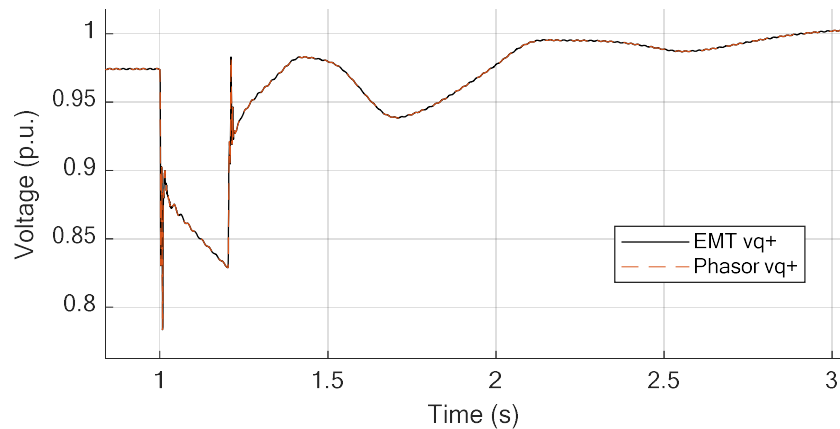


Figure 78 - Converter voltage magnitude during a symmetrical fault. VSC connected.

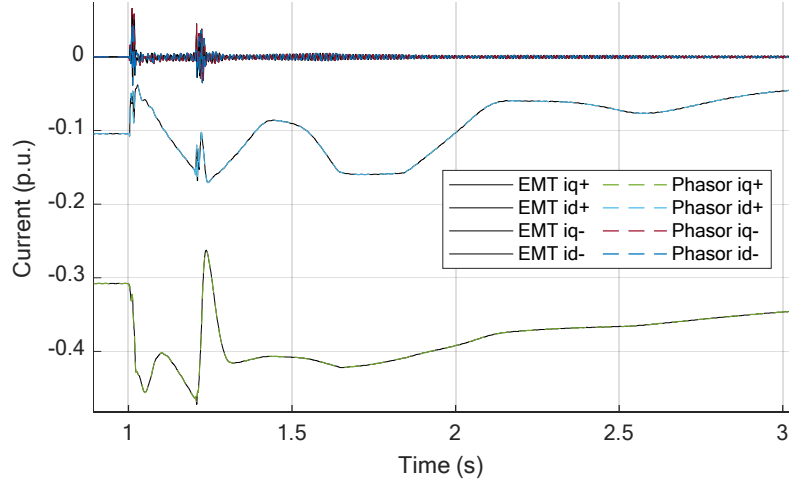


Figure 79 - Converter positive and negative sequence dq currents during a symmetrical fault. VSC connected.

During the tests, the converter triggered the LVRT characteristic which presented similar behaviour in both Phasor and EMT models.

5.4 Asymmetrical fault

In this test, a temporary $5\ \Omega$ mono-phase fault was applied at the Phase B of Bus 4 at $t = 1\ s$.

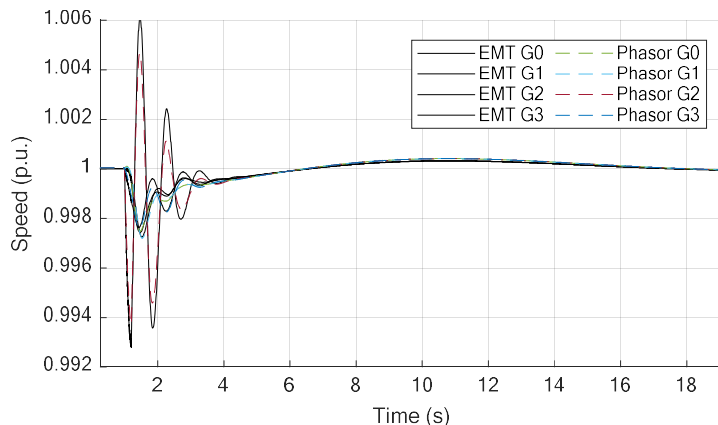


Figure 80 - SMs speeds during an asymmetrical fault. VSC connected.

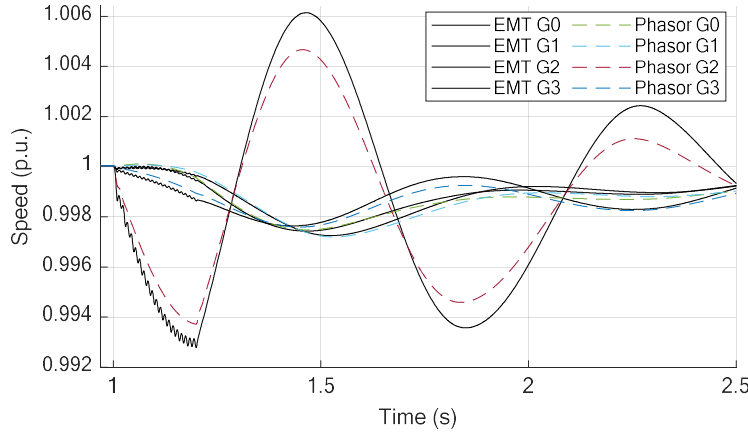


Figure 81 - SMs speeds during an asymmetrical fault (detail). VSC connected.

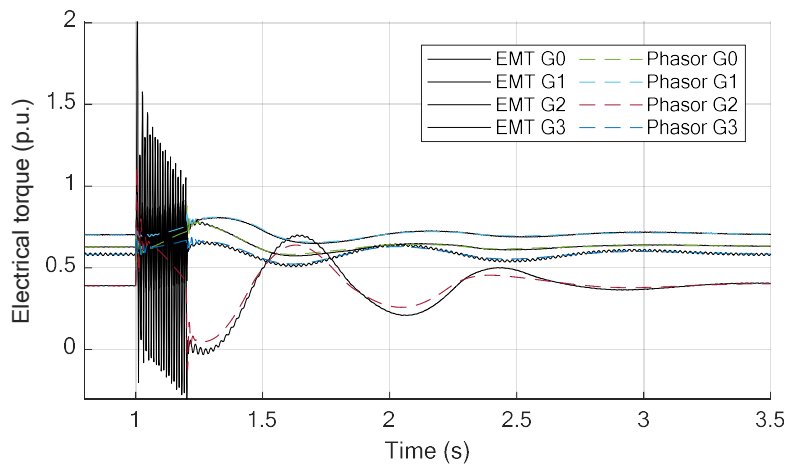


Figure 82 - SMs torques during an asymmetrical fault (detail). VSC connected.

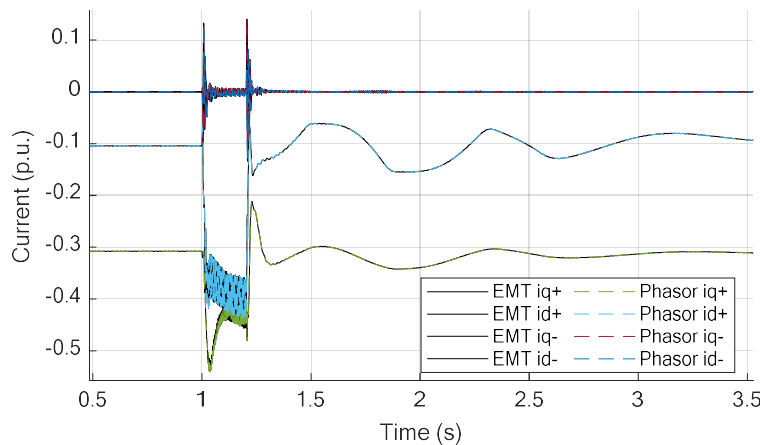


Figure 83 - Converter positive and negative sequence dq currents during an asymmetrical fault. VSC connected.

An asymmetrical fault resulted in bigger deviations of the SMs variables when compared to the symmetrical fault. Regarding the VSC, similar results were obtained for the negative sequence current control.

5.5 Line outage

In this test, a permanent solid three-phase fault was applied to the beginning of line 8 (close to Bus 1), lasting 100 ms, followed by the elimination of the fault by removing line 8.

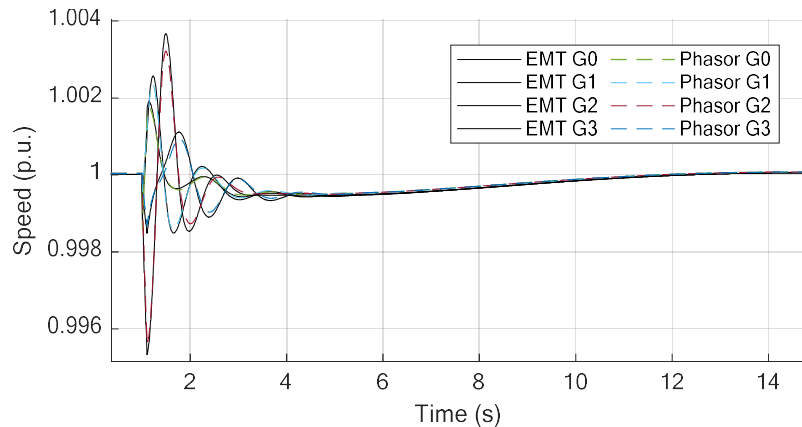


Figure 84 - SMs speeds during a line outage. VSC connected.

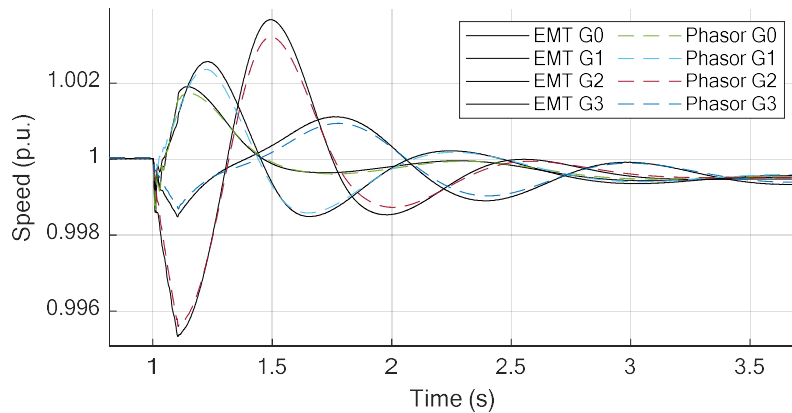


Figure 85 - SMs speeds during a line outage (detail). VSC connected.

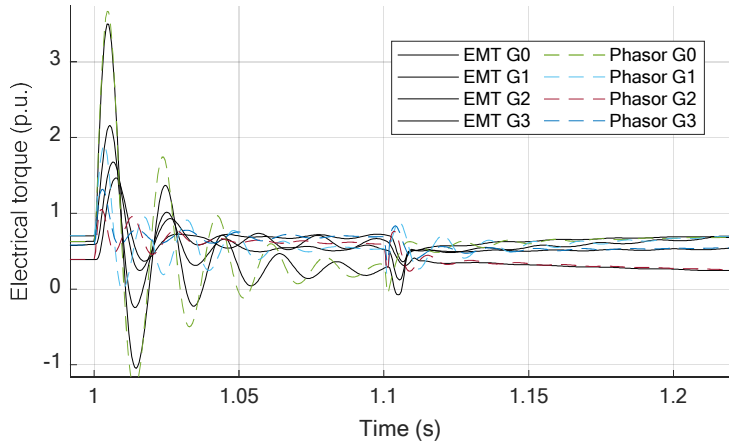


Figure 86 - SMs torques during a line outage (detail). VSC connected.

This test was similar to the case without VSC. As the system was operating with light load, no stability issues were observed.

6 References

- [1] A. Morched, B. Gustavsen and M. Tartibi, "A universal model for accurate calculation of electromagnetic transients on overhead lines and underground cables," *IEEE Transactions on Power Delivery*, vol. 14, no. 3, pp. 1032-1038, 1999.
- [2] B. Gustavsen, "Wide Band Modeling of Power Transformers," *IEEE Transactions on Power Delivery*, vol. 19, no. 1, pp. 414-422, 2004.
- [3] P. Chowdhuri, "Power System Transients," in *The Electric Power Engineering Handbook*, Boca Raton, CRC Press LLC, 2001.
- [4] N. Watson and J. Arriaga, *Power Systems Electromagnetic Transients Simulation*, 2nd ed., IET, 2018.
- [5] H. W. Dommel, "Digital computer solution of electromagnetic transients in single- and multiphase networks," *IEEE Transactions on Power Apparatus and Systems*, vol. 88, no. 2, pp. 734-741, 1969.
- [6] H. W. Dommel, *Electromagnetic Transients Program Reference Manual: EMTP Theory Book*, Portland: Bonneville Power Administration, 1986.
- [7] J. A. Martinez-Velasco, *Transient analysis of power systems : solution techniques, tools, and applications*, John Wiley & Sons, 2015.
- [8] A. Ametani, *Numerical Analysis of Power System Transients and Dynamics*, London: The Institution of Engineering and Technology (IET), 2015.
- [9] A. A. Sallam and O. P. Malik, *Power System Stability: Modelling, analysis and control*, London: IET, 2015.
- [10] IEEE, Std 1110 - *IEEE Guide for Synchronous Generator Modeling Practices and Parameter Verification with Applications in Power System Stability Analyses*, IEEE, 2019.
- [11] IEEE Std 1110-2019, *IEEE Guide for Synchronous Generator Modeling Practices and Parameter Verification with Applications in Power System Stability Analyses*, 2019.
- [12] IEEE, *Technical Report: Dynamic Models for Turbine-Governors in Power System Studies*, IEEE-PES, 2013.
- [13] IEEE, Std 421.5-2005 - *IEEE Recommended Practice for Excitation System Models for Power System Stability Studies*, IEEE, 2005.

[14] ENTSO-E, "Documentation on Controller Tests in Test Grid Configurations," 2013.